Cellular metabolic state controls mitochondrial RNA kinetics

Sean D. Reardon[1*], Clarisa Bautista[1], Shannon C. Cole[1], Julien Cicero[2], and Tatiana V. Mishanina[1*]

[1]Department of Chemistry and Biochemistry University of California, San Diego, 9500 Gilman Dr, La Jolla, CA 92093
[2]Department of Cell and Developmental Biology University of California, San Diego, 9500 Gilman Dr, La Jolla, CA 92093

*Address correspondence to: sreardon@ucsd.edu, tmishanina@ucsd.edu

Abbreviations:

mtDNA, mitochondrial DNA

mtRNA, mitochondrial RNA

OXPHOS, oxidative phosphorylation

ISR, integrated stress response

BHB, β-hydroxybutyrate

Abstract

Human mitochondrial genome encodes essential genes for the oxidative phosphorylation (OXPHOS) complexes. These genes must be transcribed and translated in coordination with nuclear-encoded OXPHOS components to ensure correct stoichiometry during OXPHOS complex assembly in the mitochondria. While much is known about nuclear gene regulation during metabolic stresses like glucose deprivation, little is known about the accompanying transcriptional response in mitochondria. Using microscopy, roadblocking qPCR, and transcriptomics, we studied mitochondrial transcription in cells subjected to glucose deprivation, which is known to cause nuclear transcription downregulation and to activate the unfolded protein response (UPR). We found that glucose deprivation stabilizes mitochondrial RNAs and slows mitochondrial transcription, effects that are quickly reversed with glucose reintroduction. Although transcriptomics revealed strong upregulation of the UPR, mitochondrial RNA stabilization was not upregulated by pharmacological activation of the UPR, but was promoted by inhibition of glycolysis, unveiling a direct connection between metabolism and regulation of mitochondrial gene expression.

Introduction

The mitochondria in eukaryotic organisms contribute the majority of cellular ATP through OXPHOS. Mitochondria contain multiple copies of their own genome and their own ribosomes, which must coordinate with the nuclear genome and cytosolic ribosomes to ensure the correct stoichiometry of the OXPHOS complex proteins synthesized in the cytosol and mitochondrial matrix[1,2]. Incorrect stoichiometry of OXPHOS proteins results

in the activation of the unfolded protein response (UPR) and cell sensitivity to proteosome inhibition[1]. Thus, coordination between the nuclear and mitochondrial genomes is essential to cellular health. The human mitochondrial genome (mtDNA) is a ~16 kb circular DNA encoding 13 essential OXPHOS complex proteins, 22 tRNAs, and 2 rRNAs (Fig. 1A). The mtDNA is entirely maintained, transcribed, and replicated by nuclear-encoded proteins[3], with transcription of human mtDNA carried out by the mitochondrial RNA polymerase (POLRMT) and the transcription factors: Mitochondrial Transcription Factor A (TFAM), Mitochondrial Transcription Factor 2B (TFB2M), and the Mitochondrial Transcription Elongation Factor (TEFM)[4–6]. Of these factors, TFAM also compacts individual mtDNA molecules into nucleoids, and TFAM concentration is thought to affect the accessibility of mtDNA for processes like transcription and replication[7–10].

Mitochondrial RNA (mtRNA) is synthesized as a polycistronic transcript from 3 promoters, the heavy strand promoter (HSP) and light strand promoters 1 and 2 (LSP1 and LSP2), located within the non-coding region of mtDNA (Fig. 1A). Recent studies demonstrated that mitochondrial mRNA transcripts are ~100-fold more abundant than nuclear OXPHOS-encoding mRNAs, are rapidly processed co-transcriptionally, and found as residents of a cellular body separate from mtDNA known as the mitochondrial RNA granule (MRG)[11,12]. mtRNA is both synthesized and degraded much more quickly than nuclear RNA, with mtRNA stability mainly determined by the Leucine-Rich Pentatricopeptide Repeat Containing protein (LRPPRC)[12]. Both mtRNA synthesis and degradation are ATP-dependent[6,13], making rapid mtRNA kinetics an energy-expensive process for the cell. Finally, mtDNA replication is dependent on mitochondrial transcription where the terminated RNA transcript from LSP1 primes replication of the

heavy mtDNA strand (Fig. 1A), although it is not known if full-length mtDNA transcription and replication are mutually exclusive on the same mtDNA nucleoid or what factors may regulate these processes[14,15].

Major progress has been made in classifying the machinery and kinetics that dictate mitochondrial transcription and replication in standard cell culture conditions of abundant glucose. However, questions remain about how metabolic changes, like a shift from a glycolytic to an oxidative metabolism, or metabolic stress like glucose deprivation, may impact mitochondrial transcription and replication processes in the short term.

Here, we sought to determine short-term (4-12 hours, h) effects of metabolic stress on mitochondrial transcription and mtDNA replication in cells cultured under glucose deprivation, with and without supplementation of alternative carbon sources. Specifically, we compared cells grown in Dulbecco's Modified Eagle Medium (DMEM) without an extra carbon source; substituting glucose with galactose, a traditional way to test OXPHOS function[16], or substituting glucose with β-hydroxybutyrate (BHB), the most abundant ketone body in mammals used as an alternative fuel during fasting, prolonged exercise, or when subject to a ketogenic diet (Fig. 1B; NG, NGGal, and NGBHB, respectively)[17,18]. Galactose can enter glycolysis through the Lenior pathway but is considered a poor glycolytic substrate, leading cells to shift to OXPHOS[19] (Fig. 1C). BHB is a four-carbon short-chain fatty acid produced predominantly in the liver when glucose becomes scarce in mammals. BHB circulates through the blood to other organs, most notably the brain, to support their continued function through oxidative metabolism[18]. As a fuel, BHB enters cells and is first broken down within mitochondria by BHB dehydrogenase to acetoacetate, then to acetoacetyl-CoA by 3-ketoacyl-CoA transferase

and finally into two acetyl-CoA molecules, which can enter citric acid cycle to supply reducing equivalents for OXPHOS. Recent work showed that BHB indeed increases ATP levels in neurons, suggesting that it is directly used as a carbon source[20]. All three conditions shift energy production from glycolysis to OXPHOS to maintain constant cellular concentration of ATP ([ATP]) short-term (Fig. 1C and S1A).

Importantly, a lack of glucose causes unfolded proteins to accumulate in the endoplasmic reticulum (ER), triggering ER stress and the integrated stress response (ISR), a cellular program facilitating several adaptations to conserve ATP and keep cells alive including slowed global translation, upregulation of OXPHOS, and selective transcription of genes aimed at maintaining cellular energy homeostasis and protein folding[16,21,22]. The ISR utilizes several key transcription factors (ATF4, DDIT3, and ATF6B), all of which are upregulated at the transcript level in our conditions as evident from the RNA sequencing (RNA-seq) analysis of 12 h NG and NGBHB treated samples. Additionally, Gene Ontology (GO) term enrichment of differentially expressed genes shows upregulation of ER stress-related genes and downregulation of genes related to cell proliferation (Fig. S1B-S1E). These results are complemented by the halt in cell proliferation in our conditions but maintained cell viability, indicative of an adaptive ISR (Fig. S1F and S1G).

Figure 1.

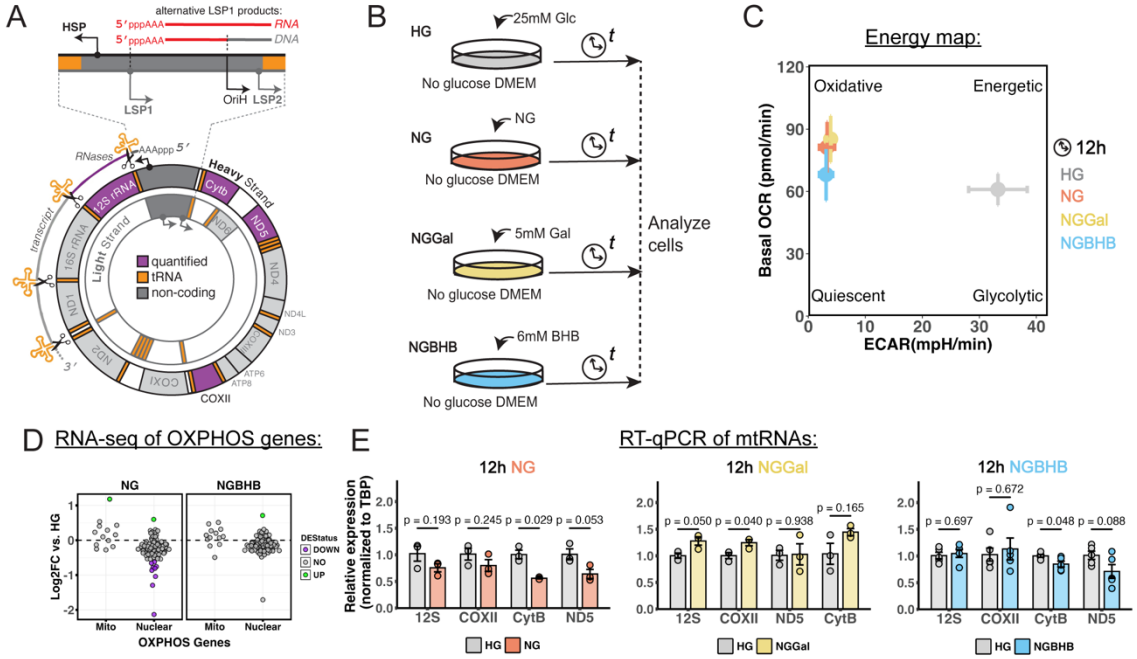

Figure 1. Media manipulations in this study and their consequences to cellular processes. A) Depiction of the human mitochondrial DNA with genes encoded by the heavy strand shown on the outside and genes encoded by the light strand on the inside. Mitochondrial genes quantified throughout this study are highlighted in purple. **B)** Schematic of color-coded cell treatments used throughout the study. **C)** Energy map of HEK293T cells deprived of glucose for 12 h showing the shift to oxidative metabolism. Data are from a Seahorse extracellular flux assay, with 10 wells per condition. **D)** RNA-seq based $\log_2$ fold-change in expression of nuclear and mitochondrially encoded OXPHOS proteins after a 12 h NG or NGBHB treatment, compared to HG. Points represent individual genes with green as upregulated, grey as non-significant, and purple as downregulated (n = 3 biological replicates). **E)** Quantitative PCR (qPCR) analysis of representative mitochondrial transcripts shows steady pools of these RNAs after 12 h of glucose deprivation (n = 3-5 biological replicates, normalized to tata-box-binding protein (TBP), data are means ± S.E.M. and associated *p* values).

Using the above glucose deprivation conditions, with a backdrop of an energetic crisis and adaptive ISR, we provide a timeline for fine-tuned mitochondrial gene expression. We show that cellular energetic status and specifically decreased mitochondrial [ATP] coincides with a slowdown in mtRNA synthesis and degradation, but that a steady-state pool of mtRNA is maintained. Strikingly, this effect is glucose-

dependent and fully reversible upon re-introduction of glucose, confirming a long-held hypothesis that mitochondrial transcription senses the metabolic status of the cell. We find that the slowdown in mtRNA degradation and synthesis observed under glucose deprivation is reproduced in nutrient abundance by direct inhibition of glycolysis but not pharmacological induction of ISR signaling. Finally, we show that the slowdown in mtRNA degradation and mitochondrial transcription is largely independent of changes in mtDNA replication, with the exception of the combined glucose deprivation and BHB supplementation where mtDNA replication was stimulated only in HEK293T cells. Our study provides evidence that mitochondrial transcription and mtRNA degradation processes sense the cellular energetic status to tune the lives of mitochondrial transcripts in the face of metabolic stress.

Results

Glucose deprivation decreases nuclear-encoded OXPHOS subunit transcripts and stabilizes mature mitochondrial RNAs

In light of the need to conserve energy under glucose deprivation and the ~100-fold mismatch between nuclear vs mitochondrial OXPHOS subunit mRNA expression, we expected to see drastic changes in mitochondrial gene expression under glucose deprivation. Fold-change analysis from RNA-seq of nuclear-encoded OXPHOS subunits showed a general downregulation in both NG and NGBHB conditions compared to HG, with a stronger effect in NG (Fig. 1D). However, fold-changes for mitochondrially encoded OXPHOS genes did not show such a general downregulation (Fig. 1D), consistent with other studies using substitution of glucose with galactose[16,23]. We confirmed the

unchanged steady-state pools of mtDNA-encoded transcripts, using whole-cell RNA-seq analysis and reverse-transcription quantitative PCR (RT-qPCR) of representative mtRNAs (purple genes in Fig. 1A and data in Fig. 1F) against the TATA-box Binding Protein (TBP). This observation is consistent with previously published studies that treated cells with galactose[16,23]. Cells thus maintain a steady pool of mtRNAs during glucose deprivation. Given the energetic burden to sustain large excess of mitochondrial transcripts over the nuclear OXPHOS transcripts (100:1, Fig. S1H), we chose to analyze mtRNA kinetics (i.e., RNA synthesis vs degradation) as a possible regulatory point.

To probe the kinetics of the steady-state pools of mtRNA, we deployed a recently reported roadblocking qPCR strategy to measure relative turnover of individual mtRNA transcripts between media conditions[24]. With this technique, the newly synthesized RNA is metabolically labelled with the uridine analog 4-thiouridine (4sU), whereas the unlabeled RNA reports on the pre-existing transcripts prior to labelling (Fig. 2A). Cells are treated with 4sU for a given time, and total RNA is purified and treated with *N*-ethylmaleimide (NEM) to alkylate the sulfhydryl group on the 4sU incorporated into RNA. These alkylated bases interrupt complementary DNA (cDNA) synthesis during the reverse transcription step of qPCR sample preparation, while full-length cDNA of unlabeled transcripts is synthesized. The resulting cDNA is then used to compare the relative unlabeled RNA between conditions normalized by a synthetic spike-in RNA control. The qPCR signal allows relative comparisons of RNA turnover between conditions or timepoints, where the signal reports on the unlabeled (older) RNA of interest

(Fig. 2B). Using this technique, we chose to label for the last 2 h of each treatment using a final concentration of 50 μM 4sU, a concentration known to limit 4sU toxic effects[25].

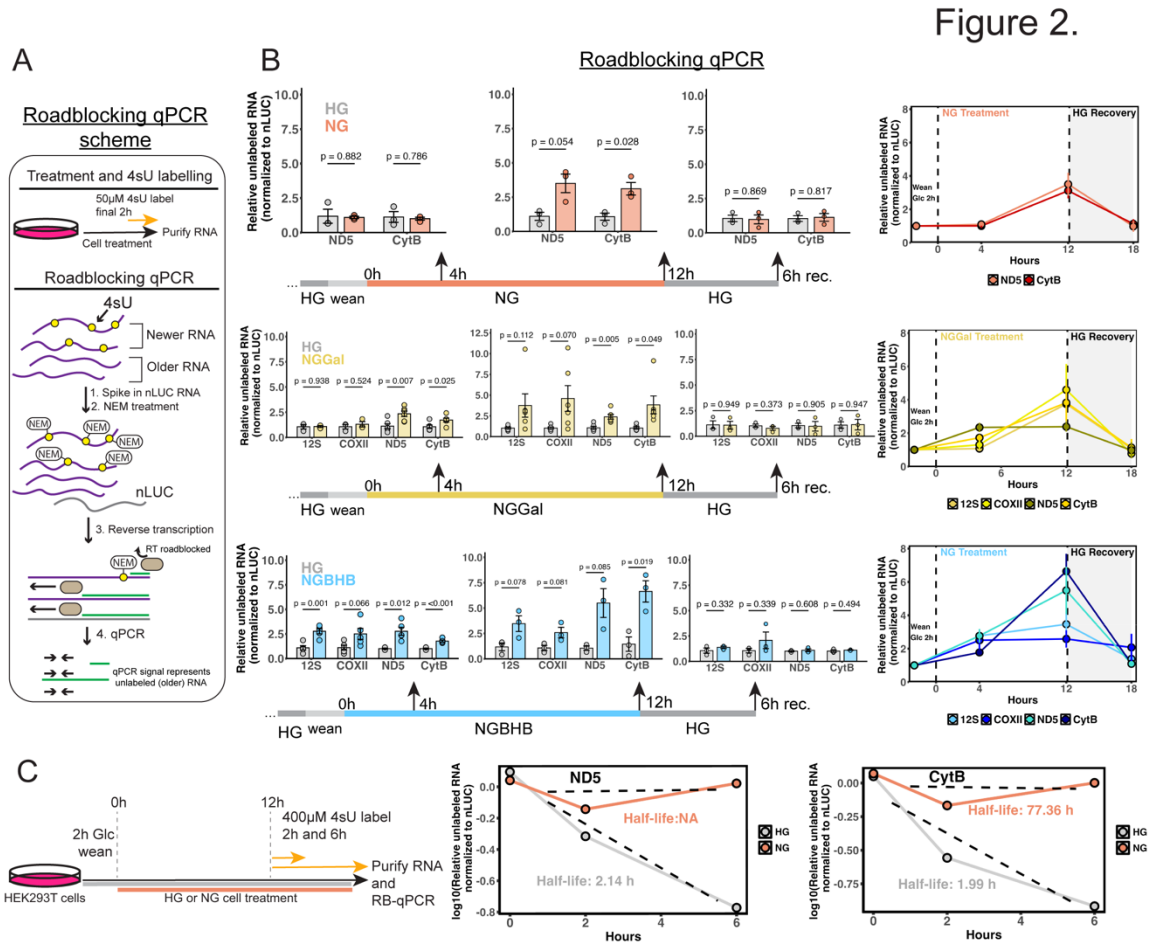

Figure 2. Mitochondrial RNA kinetics under different glucose deprivation conditions. A) General schematic of the roadblocking qPCR approach to measure RNA stability. **B)** Comparative roadblocking qPCR analysis of mitochondrial transcripts shows an increase in unlabeled RNA over time upon glucose deprivation. In NG- and NGBHB-treated cells subjected to a 6-h recovery in HG, unlabeled RNA levels returned to those observed in HG (n = 3-6 biological replicates, two-tailed Student's *t*-test, data are means ± S.E.M. and associated *p* values). **C)** Representative mitochondrial RNA half-life measurements by roadblocking qPCR. Each dot on the plots represents the average of 3 biological replicates at different 4sU pulse times after a 12 h treatment (line-of-best-fit is shown as a dotted line and half-life values are displayed).

We observed a higher amount of unlabeled RNA upon glucose deprivation for mitochondrial transcripts ND5 and CytB after 12 h in all conditions (Fig. 2B). This implies a slowdown of mtRNA degradation and stabilization of older transcripts. Interestingly, while NG did not lead to accumulation of older RNA until 12 h into the treatment, NGGal and NGBHB treatment as short as 4 h showed a significant buildup of unlabeled RNA compared to HG (Fig. 2B). Additionally, we saw the highest degree of stabilization for ND5 and CytB transcripts in NGGal and NGBHB conditions compared to HG, while COXII was stabilized to a lesser degree and 12S ribosomal RNA only showed slight stabilization in the NGBHB condition compared to HG (Fig. 2B). To ask whether this decrease in mtRNA turnover was reversible, we cultured cells for 12 h in each condition before swapping the media back to high (25 mM) glucose without BHB for 6 h, followed by 4sU labelling during the final 2 h of growth. Strikingly, the unlabeled RNA at the end of the 6 h swap back to HG matched that of the HG control, indicating that mtRNA turnover is highly sensitive to the availability of glucose and recoverable on a relatively short time scale (Fig. 2B) In addition, we noted a similar accumulation of unlabeled RNA after a 12 h NG growth compared to HG in HepG2 cells, demonstrating a conserved mtRNA stabilization response to glucose deprivation (Fig. S2A).

The higher roadblocking qPCR signal in glucose-deprived cells (Fig. 2B) could be due to slower mitochondrial transcription (see the next section), i.e., less 4sU incorporation into mtRNA and thus less roadblocking during the RT step. To rule out changes in the rate of mitochondrial transcription as the cause of unlabeled RNA accumulation, we performed a complementary roadblocking qPCR experiment in which cells were starved of glucose for longer (12 h) prior to the 4sU addition, with 4sU-labeled

samples analyzed at the 0, 2 and 6 h marks post-4sU addition and signal compared to the 0 h timepoint in each given condition (immediately before 4sU addition). This approach gives time for mitochondrial transcription rate to reach equilibrium under the given metabolic condition before the 4sU introduction, allowing the decay in signal to represent mitochondrial turnover alone. We noted the expected decrease in signal for the ND5 and CytB transcripts in HG, indicative of mtRNA decay (Fig. 2C and S2B). Linear regression of log-transformed relative values yielded half-life measurements of ~2 h for each transcript, in line with recent reports of mtRNA half-lives[12]. Strikingly, we did not observe the same decay pattern for either transcript in cells cultured in NG and extremely extended half-lives for each transcript (Fig. 2C and S2B). As a control, we measured the decay of the mitochondrial 12S ribosomal RNA in HG, which is expected to display a much longer half-life (~15 h) compared to the coding transcripts (Fig. S2C)[12,26]. These results establish that mitochondrial transcripts are stabilized during glucose deprivation and that roadblocking qPCR can accurately measure these changes.

Mitochondrial transcription slows upon glucose deprivation

The surprising result that mtRNA turnover in cells slowed (older mtRNAs accumulated) but the steady-state pools of mtRNAs remained the same or slightly decreased upon glucose removal implies that mtRNA synthesis must slow down under these conditions. To confirm this experimentally, we employed pulse-chase immunofluorescence imaging with staining against the uridine analog bromouridine (BrU). BrU is incorporated into mtRNA during a short “pulse” of the analog and appears as puncta within the MRG upon anti-Br(d)U antibody staining (Fig. 3A). BrU in the media is then replaced with a large excess of uridine; thus, any *de novo* transcripts made during

this “chase” phase will no longer contain BrU and be invisible in the anti-BrU channel. Two pieces of information can be extracted from such a pulse-chase assay: (i) anti-BrU signal intensity at the end of the pulse gives a sense of transcription rate (higher signal corresponds to higher rate of nucleotide addition); (ii) anti-BrU signal remaining after the chase informs on the composite rate of transcription initiation and RNA degradation (higher persisting anti-BrU signal in the presence of uridine competitor suggests slower transcription initiation and/or slower BrU-labeled RNA degradation). The difference between the two values yields an estimated “chase rate”, which represents the rate of RNA degradation.

We chose to compare the HG to NG and NGBHB treatments due to the NGBHB’s pronounced mtRNA turnover phenotype on the shortest timescale (Fig. 2B). Briefly, the cells were cultured in HG or NGBHB for 90 min then pulsed with BrU for 30 min, followed by a 2 h chase with uridine. Cells were immunostained and imaged using confocal microscopy both after the pulse and at the end of the chase (Fig. 3A). From Z-projections, we used image segmentation to quantify extranuclear BrU intensity per cell (Fig. S3A). We observed that NG and NGBHB-cultured cells incorporated significantly less BrU into their mtRNA during the pulse than HG-cultured cells, indicative of slower transcription in after 90 min of treatment (Fig. 3B, note: NGBHB reps 1 and 2 were stained slightly differently so data is shown separately). Despite this difference in the starting BrU-labeled mtRNA, both HG- and NG/NGBHB-grown cells “chased” to a similar same level (Fig. 3A, 3B and S3B). This suggests that mtRNA turnover (composite rate of *de novo* synthesis and degradation) slowed in NG and NGBHB, as indicated by the “chase rate” calculated as the difference between the average pulse and chase value in a given condition (Fig.

3C). From segmented regions of interest (ROIs), we observed no changes in translocase of outer mitochondrial membrane (TOMM20) signal across these conditions, validating that our anti-BrU signal derived from generally equal mitochondrial content (Fig. S3C).

Figure 3.

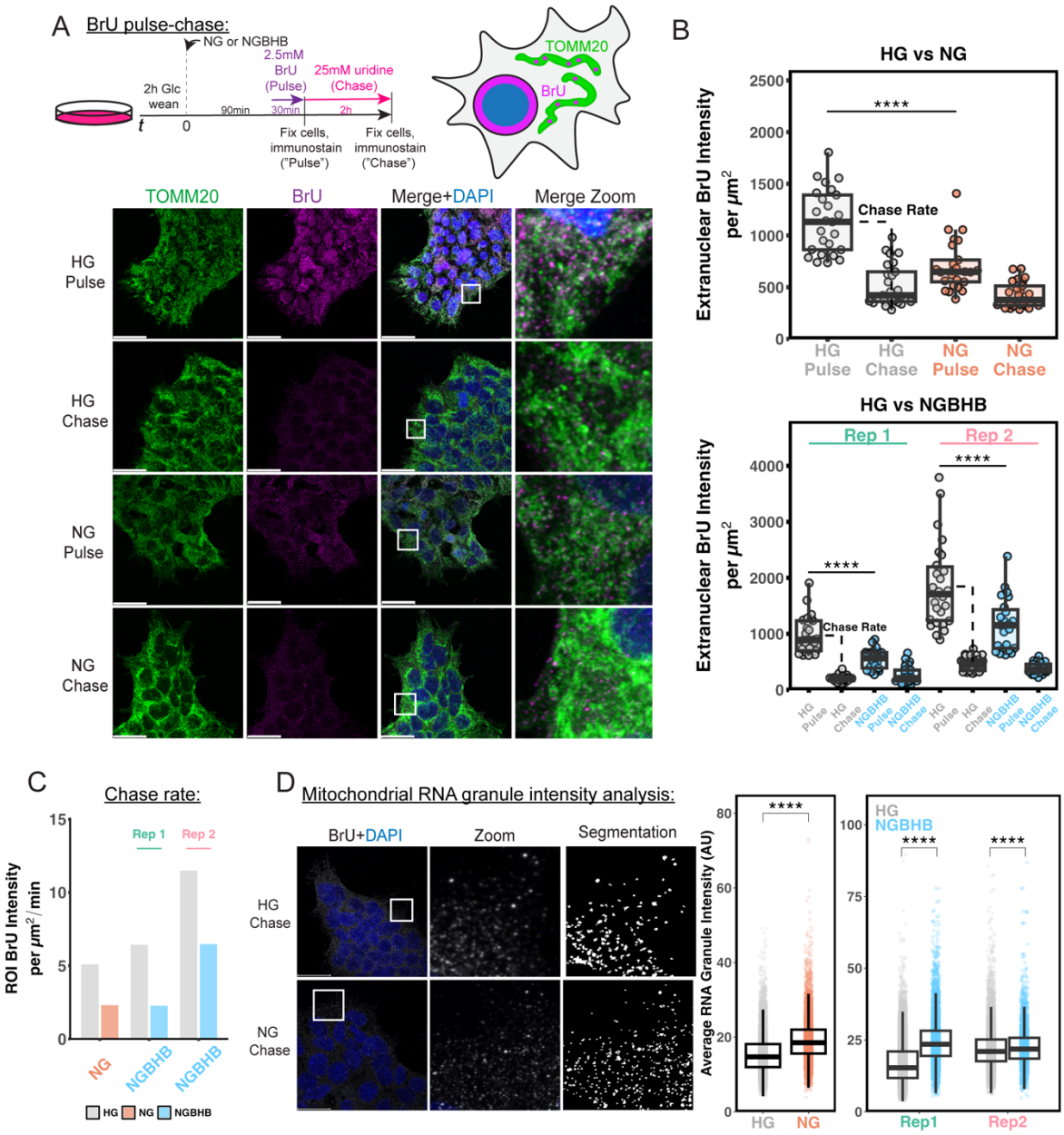

Figure 3. Pulse-chase experiments to visualize changes in mitochondrial transcription rate upon glucose deprivation. A) Schematic of a bromouridine (BrU) pulse-chase assay (left) and staining (right). HEK293T cells were cultured in HG, NG, or

NGBHB for 90 min before a 30-min BrU pulse, after which portion of cells was fixed for immunofluorescence ("pulse" samples) to assess transcription rate. Remaining cells were then chased with 25 mM uridine for 2 h and fixed for immunofluorescence ("chase" samples) to assess RNA degradation rate. Representative images (bottom) are maximum intensity projections for HG vs. NG treated cells stained against TOMM20 (mitochondria) and BrU (newly synthesized RNA). Scale bar = 30 μm. **B)** Quantification of extranuclear BrU intensity per cell for pulse and chase samples of HG vs NG (top), and HG vs. NGBHB (bottom, ****$p < 0.0001$, one-way ANOVA with Tukey's multiple comparisons correction; n=50 cells per replicate, with 25 cells in each condition quantified, data represents individual cells and bars represent median, boxes represent the 1st and 3rd quartiles, and whiskers are no further than 1.5 times the interquartile range). **C)** Quantification of BrU intensity chase rate, calculated as (avg. pulse - avg chase)/120 min using data from 3B NG and NGBHB samples. **D)** Maximum intensity projection chase images for HG and NG treated cells, and segmented mitochondrial RNA granules (left, MRGs) for quantification of average pixel intensity per MRG from samples in 3B (right, ****$p<0.001$, Wilcoxon rank sum test, data represent individual MRGs and box representation as above).

These data complement the increased mtRNA stability in NG and NGBHB vs HG gleaned from 4sU roadblocking qPCR analysis (Fig. 2B) and establish that mitochondrial transcription rate is lower in an NG and NGBHB vs HG culture. As an additional support for slowed mitochondrial transcription, we saw a downward trend for the LSP1 primer synthesis by qPCR at 12 h of NGBHB treatment (Fig. S3B). A recently characterized mitochondrial non-coding RNA, the 7S RNA, has been shown to directly inhibit POLRMT in cells and *in vitro*[27]. To rule out the possibility of mitochondrial transcription inhibition by the 7S RNA, we measured abundance of the mitochondrial 7S RNA with qPCR and found no difference in 7S RNA levels between HG and NGBHB conditions (even at 12 h of treatment), likely ruling the 7S RNA out as a cause for the observed decrease in transcription rate and further evidence of stabilized RNA pools (Fig. S3B).

When analyzing the chase images, we noticed that the NG and NGBHB images contained particularly bright MRGs compared to HG treatment, even though whole-cell anti-BrU intensity was "chased" to the same level overall in the two conditions. To capture

this further, we segmented the chase images to measure the average pixel intensity per MRG (Fig. 3D, left and S3E). While many MRGs in HG and NGBHB chased to the same low intensity, there was a significant bright population of MRGs in the NG and NGBHB chase samples (Fig. 3D, right). We hypothesize that these bright MRGs could represent a slower flux of newly synthesized RNAs out of MRGs or the recently described “storage” granules for mtRNAs during stress, such as pharmacological inhibition of mitochondrial transcription or toxic RNA buildup[28,29]. Taken together, these data support slowed mtRNA synthesis and potential changes to mtRNA flux from MRGs or mtRNA sequestration through metabolic stress (e.g., scarcity of glucose).

Mitochondrial degradosome protein levels and localization to mitochondria are maintained during glucose deprivation

To determine if slowed mtRNA turnover in glucose-deprived cells was caused by altered levels of the proteins that dictate mtRNA stability and degradation, we first performed whole-cell western blot analysis of these proteins. Specifically, we blotted against the mtRNA chaperone LRPPRC and proteins important for mtRNA degradation (G-Rich RNA sequence binding factor 1, GRSF1; ATP-dependent RNA helicase SUPV3L1, SUV3; Polynucleotide Phosphorylase, PNPT1). None of these proteins showed any changes when subject to 12 h glucose deprivation compared to HG (Fig. S4A).

Figure 4.

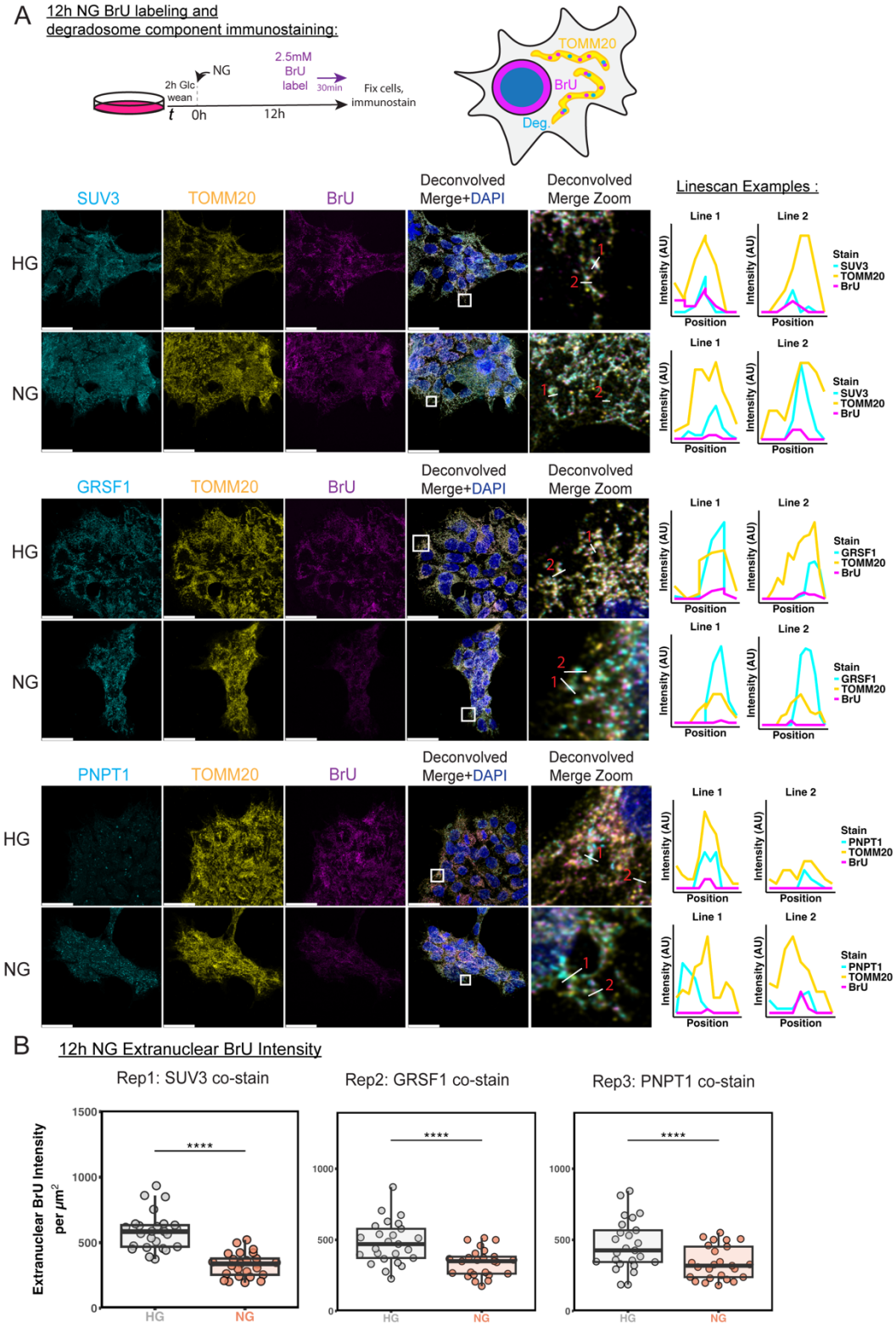

Figure 4. Mitochondrial degradosome proteins localize to mitochondria. A) Schematic of a bromouridine (BrU) incorporation assay (left) and staining (right) of

TOMM20, BrU, and mitochondrial degradosome components (Deg). HEK293T cells were cultured in HG, or NG for 11.5 hours before a 30-min BrU pulse, after which portion of cells was fixed for immunofluorescence. Representative images are shown as raw channel max intensity projections and a deconvolved merge maximum intensity projection for 12 h HG vs. NG treated cells stained against TOMM20 (yellow, mitochondria), BrU (magenta, newly synthesized RNA), and mitochondrial degradosome components SUV3, GRSF1, and PNPT1 (Cyan). Scale bar = 30 μm. To the right of each image set are two example line-scans representing raw image intensities for each channel. **B)** Quantification of extranuclear BrU intensity per cell for 12 h HG vs NG BrU pulse samples in A (****$p < 0.0001$, two-tailed Student's *t*-test; n=50 cells per replicate, with 25 cells in each condition quantified, data represents individual cells and bars represent median, boxes represent the 1st and 3rd quartiles, and whiskers are no further than 1.5 times the interquartile range).

We next visualized the localization of the mitochondrial degradosome proteins SUV3, GRSF1, and PNPT1 in a 12 h NG treatment compared to HG. To accomplish this, we used a similar BrU labeling to mark mtRNAs as in the previous section, followed by immunostaining against BrU, TOMM20, and each degradosome component (Fig. 4A). We did not observe any obvious changes in protein localization, as shown in example line scans from each sample (Fig. 4B), with each degradosome component still localized to mitochondria and with mtRNA. Together, these findings indicate that the mtRNA stabilization phenotype is not caused by the changes in levels or localization of mitochondrial degradosome proteins. Rather, the mtRNA turnover appears to slow down through a universal energy-sensing mechanism.

Using the same segmentation scheme for 90 min BrU-labeled MRGs as in the previous section, we measured the extranuclear BrU intensity per cell in these 12 h NG samples vs the respective HG control. We saw lower mitochondrial transcription rate in NG samples and unchanged TOMM20 intensities per ROI (Fig. 4B and S4B). These results along with those from Fig. 3B show a rapid and sustained drop but not a halt to mitochondrial transcription under glucose deprivation.

Mitochondrial transcription rate mirrors mitochondrial ATP levels

Given the quick (within ~90 min) slowdown in mtRNA production upon glucose removal and the sustained (at 12 h) drop in transcription, we wondered if this was tied to mitochondrial ATP pools. Human mitochondrial transcription is hypothesized to be especially sensitive to local [ATP], and transcription initiation rate would reflect [ATP]-dependence because the first three nucleotides in mitochondrial transcripts are all adenosines. Indeed, *in vitro* studies with purified human mitochondrial transcription initiation proteins showed slower initiation of RNA synthesis at lower [ATP][6]. Moreover, local [ATP] in the mitochondrial matrix is expected to directly affect the rate of mtRNA degradation because the helicase SUV3 that unwinds the double-stranded RNA (dsRNA) and RNA-DNA hybrids for exonuclease cleavage is ATP-dependent[13].

To assess mitochondrial ATP content after glucose removal, we turned to a previously characterized, genetically encoded and mitochondrially targeted ratiometric ATP sensor[30]. The sensor contains a circularly permuted superfolder GFP (sfGFP) between two ATP binding helices of *Bacillus subtilis* F_o-F_1 ATPase, which upon binding ATP causes an increase in sfGFP fluorescence (Fig. 5A). The C-terminus of this sensor encodes a spectrally separate red fluorescent protein miRFP670nano, which acts as a control for sensor concentration and allows the ratio of green-to-red fluorescence intensity to report on mitochondrial ATP content (Fig. 5A).

Using confocal live-cell 2D imaging and segmentation of each channel, we quantified the mitochondrial [ATP] per cell for our glucose deprivation conditions compared to HG at the 2 h and 12 h treatment marks (Fig. 5A and S5A). We saw a

significant drop in mitochondrial [ATP] in all conditions (Fig. 5B and S5B) at both timepoints with no significant differences between the glucose deprivation conditions. This was a surprising result because we expected BHB to boost mitochondrial [ATP], being a mitochondria-specific fuel. The sustained drop in mitochondrial [ATP] is an important finding, given that all glucose deprivation conditions lead cells to solely use OXPHOS for energy production (Fig. 1C), whereas HG-grown cells are both highly glycolytic and oxidative (Fig. 1C). It is possible that cells reliant on OXPHOS upregulate export of ATP from mitochondria, especially in conditions where glycolysis is shut off. Strikingly, when we compared a normalized transcription rate and mitochondrial [ATP] over our two timepoints, we saw that both dropped to a similar relative level (~50% mitochondrial [ATP] and ~60% mitochondrial transcription compared to HG) and persisted there, providing further evidence that mitochondrial transcription can respond to changes in metabolism and potentially sense compartmental [ATP] (Fig. 5C).

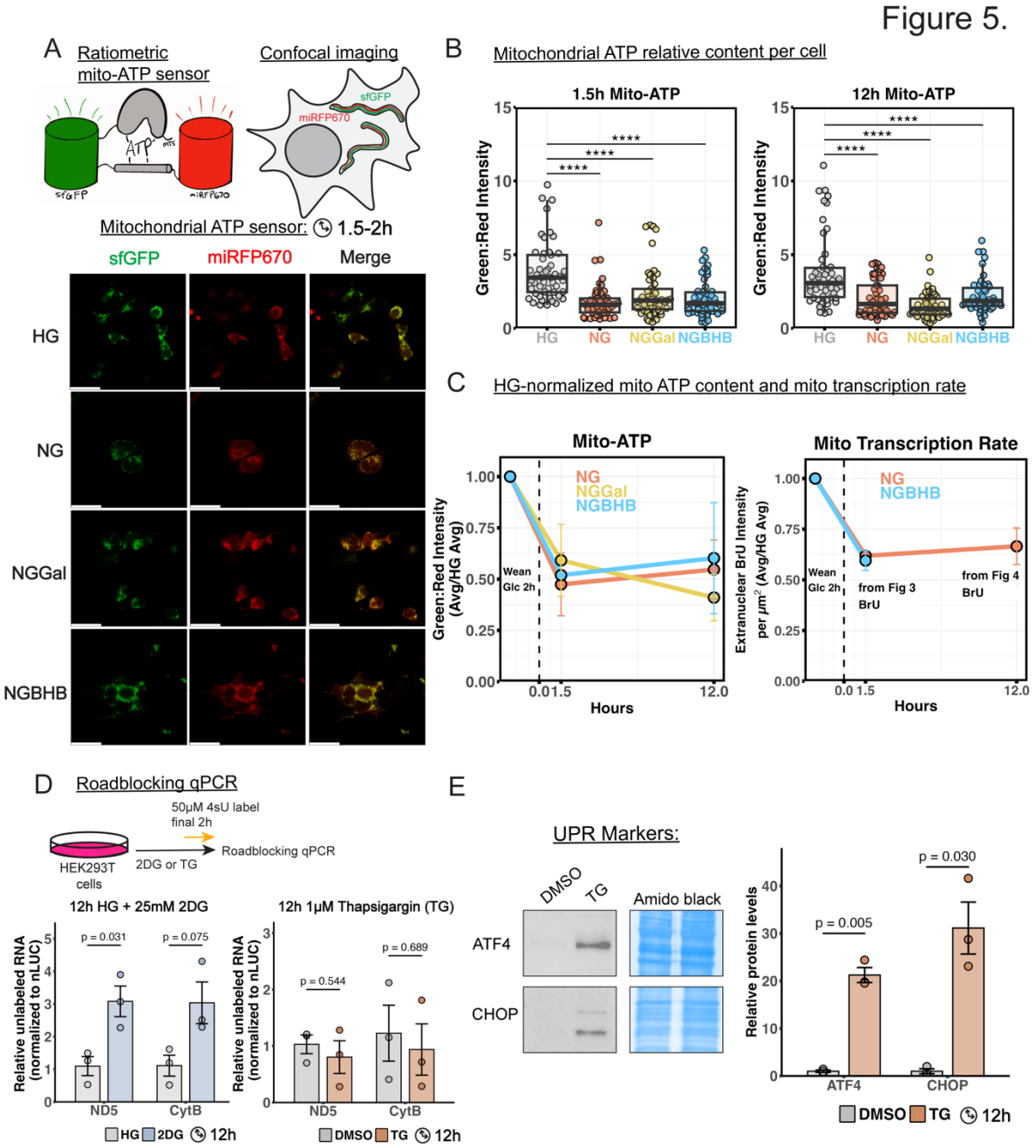

Figure 5. Mitochondrial ATP content reflects mitochondrial transcription rate. A) A cartoon showing the mitochondrial ATP sensor on the pAAV-CAG-iATPSnFR2A-95A-A119L-miRFP670nano3 plasmid (Addgene # 209723), which uses a circularly permuted sfGFP as a sensor between two ATP binding helices of *Bacillus subtilis* F_o-F_1 ATPase, and miRFP670 as a control (left). The ATP sensor is targeted to mitochondria with a mitochondrial targeting sequence (right). Representative 2D images of mitochondrial ATP sensor imaging in HEK293T cells during treatment for 1.5 h in glucose deprivation conditions (bottom). **B)** Quantification of mitochondrial ATP per cell as the ratio of green:red intensity for samples treated in each condition for 1.5 and 12 h (****p<0.0001,

one-way ANOVA with Tukey's multiple comparisons correction, n=50 cells per condition, with 25 cells in each replicated from 2 biological replicates, quantified points are individual cells and bars represent median, boxes represent the 1st and 3rd quartiles, and whiskers are no further than 1.5 times the interquartile range). **C)** Summarized timeline results from mitochondrial ATP measurements (left) and BrU pulse assays (right) as each conditions average value normalized to the respective HG value. Data represents the mean and S.E.M. for each sample. **D)** Experimental schematic and roadblocking qPCR analysis of ND5 and CytB in HEK293T cells treated in 10 mM 2DG for 12 h in the presence of high glucose or 1 μM thapsigargin (TG) for 12 h, showing RNA stabilization with 2DG treatment (n = 3 biological replicates, two-tailed Student's *t*-test, data is mean ± S.E.M. with associated *p* values). **E)** Representative western blots for analysis of ATF4 and CHOP expression in HEK293T cells treated with 1 μM thapsigargin (TG) for 12 h compared to DMSO treated (left), and quantification of blots and quantification of blots (right, n = 3 biological replicates, normalized to the average HG or DMSO values respectively, two-tailed Student's *t*-test with associated *p* values).

Given the drop in mitochondrial [ATP], we next indirectly checked on the activity of the RNA helicase SUV3 by immunostaining with the dsRNA specific antibody J2 of 12 h NG treated cells. We found a slight increase in extranuclear J2 intensity compared to HG, but not an increase on par with the degree of stabilization of mtRNAs in this condition (Fig. S5C). This could be due to the slowed transcription reducing the burden on SUV3 to unwind mitochondrial dsRNA. Most importantly, we did not see large dsRNA foci induced by long-term SUV3 ablation[31], arguing that stabilized mtRNAs are likely still traversing through the mitochondrial central dogma in our glucose deprived conditions, albeit more slowly.

Glycolytic insults but not ER-stress induced ISR signaling stabilizes mtRNA

Considering that glucose deprivation induces ISR signaling, we applied roadblocking qPCR to determine if glycolytic inhibition or direct induction of ISR signaling in nutrient abundance could recapitulate mtRNA stabilization phenotype. To directly target glycolysis, we treated HEK293T cells grown in 25 mM glucose with 25 mM 2-

deoxyglucose (2DG), which upon conversion to 2-deoxy-glucose-6-phosphate can inhibit the glycolytic enzymes hexokinase and phosphoglucose isomerase[32,33]. We indeed found that a 12 h 2DG treatment caused the stabilization of ND5 and CytB transcripts seen in glucose deprivation conditions, while steady-state qPCR shows maintained overall transcript levels (Fig. 5C and S5C). These results support the notion that inhibition of glycolysis and potentially the drop in mitochondrial [ATP] are closely tied to the mtRNA stabilization and transcription slowdown.

To test whether signaling upstream (e.g., ISR activation) of mtRNA synthesis or the downstream fate of mtRNA (translation) contributed to the observed mtRNA stabilization, we turned to pharmacological treatments that target each of these processes. To illicit direct UPR activation, we treated cells with 1 μM thapsigargin (TG), an inhibitor of the sarcoplasmic/ER Ca^{2+}-ATPase (SERCA) required for pumping Ca^{2+} into the endoplasmic or sarcoplasmic reticulum[34]. TG treatment depletes ER Ca^{2+}, leading to ER stress and the UPR[35]. Cells treated with TG did not show the ND5 or CytB transcript stabilization compared to a DMSO (vehicle)-treated control, despite activation of the UPR evident from the increased levels of ATF4 and CHOP, classic markers of UPR[21,36] (Fig. 5C, 5D and S5D). Thus, we propose that the UPR coincides with but does not necessarily lead to mtRNA stabilization and mitochondrial transcription slowdown. To directly inhibit mitochondrial translation, we treated cells with chloramphenicol, an antibiotic specific for mitoribosomes[31]. We found that chloramphenicol treatment generally left mtRNA transcript lifetimes unaffected except for destabilization of ND5 (Fig. S5E).

Mitochondrial RNA transcription rate changes and stabilization is generally independent of mtDNA replication

With the knowledge of mitochondrial transcription being absolutely required for mtDNA replication, we measured the relative mtDNA copy number (CN) under each glucose deprivation condition using RT-qPCR. In agreement with past studies[23], NG and NGGal did not change the mtDNA CN, but the NGBHB condition caused a ~2-fold increase in CN at 12 h compared to HG in HEK293T cells (Fig. 6A). We found that the NGBHB-induced CN increase persisted at 24 h in HEK293T cells but this effect was not observed in other tested cell types (HepG2, U2OS, and Mouse Embryonic Fibroblasts, MEF) (Fig. 6A). Furthermore, when HEK293T cells were treated with 6 mM BHB in the presence of high glucose (HGBHB), the increase in mtDNA CN was no longer observed, implicating *both* BHB and lack of glucose in the CN increase (Fig. 6A). Given that BHB is derived from fatty acids, we probed HEK293T cell mtDNA CN using a 12 h treatment without glucose and supplementation with one of the two most abundant fatty acids in humans, palmitic acid and oleic acid, and found no change in CN compared to HG (Fig. S6A). In light of the characterization of HEK293 lineage as a combination of liver, neuronal, and adrenergic cells[37], and the literature implicating BHB as a brain fuel during fasting, we next treated SH-SY5Y, a typical cell line used as a neuronal model, and a differentiated neural spheroid model with a physiologically feasible concentrations of low glucose (1 mM)[38] and 6 mM BHB for 12 h and observed no change in mtDNA CN compared to the HG control (Fig. S6B), further demonstrating that the NGBHB-induced increase in mtDNA CN is specific to HEK293T cells.

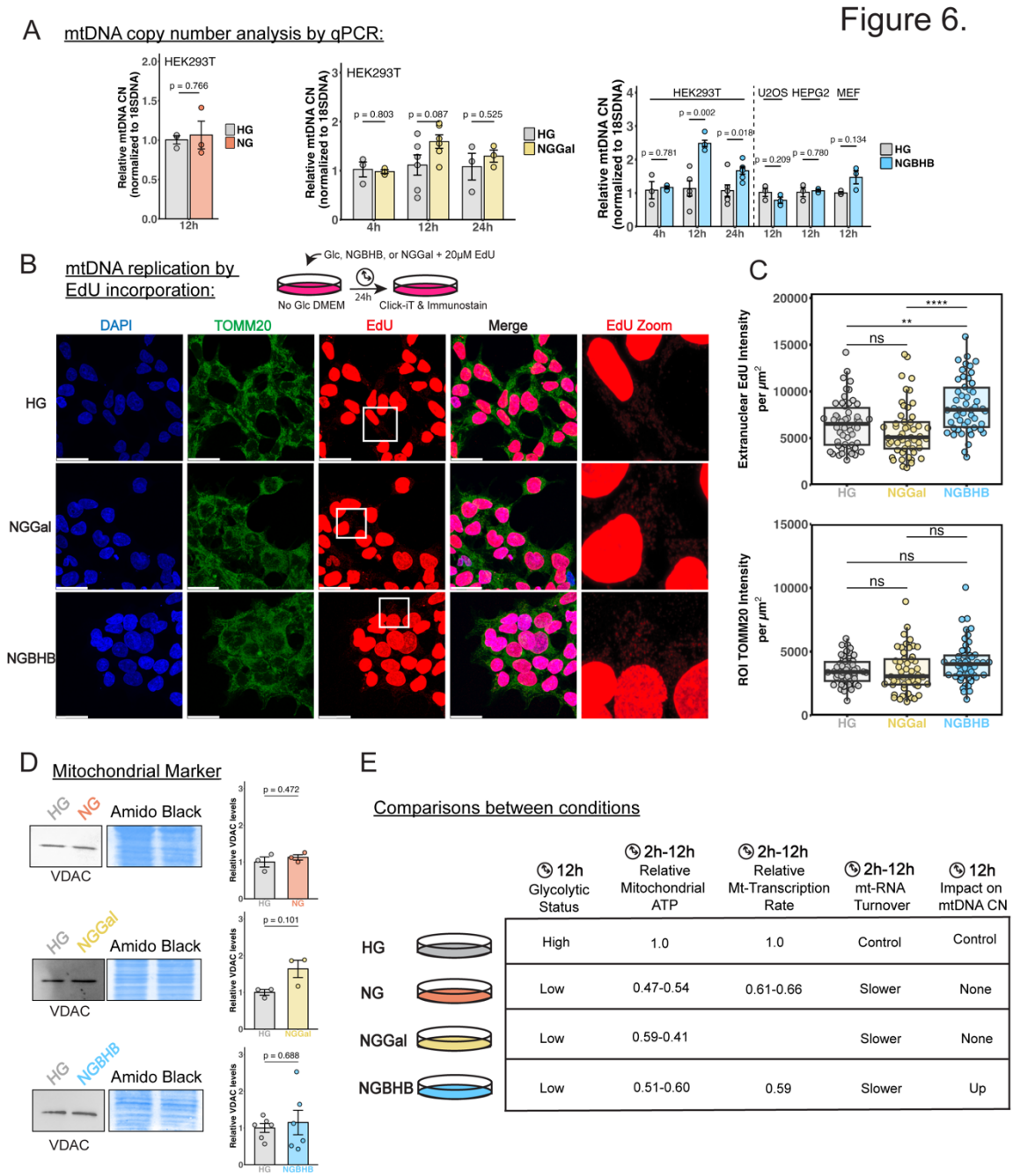

Figure 6. Combination of glucose deprivation and BHB supplementation increases mitochondrial DNA content in HEK293T cells. A) Quantitative PCR (qPCR) analysis of mtDNA copy number (CN) in high glucose (HG) and glucose deprivation conditions. mtDNA was detected with primers for CytB normalized to 18S DNA (n = 3-6 biological replicates, two-tailed Student's *t*-test, data is mean ± S.E.M. with associated *p* values). **B)** Schematic for EdU incorporation into newly synthesized DNA and immunostaining in HEK293T cells (top) and representative images as max projections (bottom; scale bar = 30 μM). **C)** Quantified extranuclear EdU intensity per cell for each condition and total TOMM20 signal per ROI as a control for mitochondrial

content (right, ns, nonsignificant; ****p <0.0001, **p<0.01, one-way ANOVA with Tukey's multiple comparisons correction, n= 50 cells: 25 cells each condition were quantified for 2 biological replicates, data represents individual cells and bars represent median, boxes represent the 1st and 3rd quartiles, and whiskers are no further than 1.5 times the interquartile range). **D)** Representative Western blots for analysis of VDAC expression in HEK293T cells treated with glucose deprivation conditions 12 h compared to HG (left), and quantification of blots and quantification of blots (right, n = 3 biological replicates, normalized to the average HG values respectively, two-tailed Student's *t*-test with associated *P* values). **F)** Summary findings for glucose deprivation's effects on metabolism, mitochondrial ATP, mitochondrial transcription rate, RNA stability, and mitochondrial DNA copy number.

To provide visual support for the increased mtDNA CN and thus increased mtDNA replication, we used metabolic labelling and immunofluorescence detection with a Click-iT 5-ethynyl 2'-deoxyuridine (EdU) Labelling kit to detect newly synthesized mtDNA (Fig. 6B). Briefly, HEK293T cells were cultured in the presence of 20 μM EdU (a synthetic nucleoside that is incorporated into newly synthesized DNA) for 24 h in the HG, NGBHB, or NGGal conditions followed by indirect immunolabelling, confocal imaging, image segmentation and quantification of extranuclear EdU signal per cell. Image analysis revealed a significant increase in newly synthesized mtDNA in the NGBHB condition compared to both the HG and NGGal (Fig. 6C and Fig. S6D), validating mtDNA CN measurements by qPCR (Fig. 6A). We found no significant difference in TOMM20 signal within our quantified ROIs, validating EdU intensity results (Fig. 6C). Importantly, western blot analysis of the voltage-dependent anion channel (VDAC) as a proxy of mitochondrial mass showed no differences after treatment with each glucose deprivation condition compared to HG (Fig. 6D), demonstrating that the increase in mtDNA CN in the NGBHB condition is independent of mitochondrial mass.

A recent study on mitochondrial nucleoid proteins found that inhibition of mitochondrial translation with chloramphenicol can stimulate mtDNA replication[39], a

response with a currently unknown mechanism but is hypothesized to be compensatory. Given the fact that the HGBHB condition did not show this response, we wondered if BHB imposes an added stress on the mitochondrial central dogma to elicit an increase in mtDNA CN. Recent reports demonstrated that BHB can post-translationally modify lysine residues on proteins in human cells as a non-canonical acylation and that modification is widespread. One study reports a primary target of this modification being the glycolytic enzyme aldolase (~39 kDa), with BHB modification inhibiting aldolase activity[40], while other reports claim a majority of KBHB is found on nuclear proteins and modifies histones directly[41,42]. In support of this recent work, we saw widespread lysine-β-hydroxybutyrylation in HEK293T cell lysates treated with NGBHB for 12 h compared to HG (Fig. S6E). Additionally, using cell fractionation and histone extraction, we detected KBHB on histone-enriched samples using anti-KBHB western blots (Fig. S6F).

We analyzed RNA-seq data to identify differentially expressed genes between 12 h NGBHB and NG treated HEK293T cells. We found very few genes to be differentially expressed but an increase in expression for genes related to steroid and cholesterol synthesis (Fig. S6G and S6H), some of which can reside in mitochondria or the ER, while others are related to transcription and the peroxisome[43–49]. This trend was also recently reported in transcriptomics of mice livers from mice subject to a ketogenic diet[40]. Intriguingly, steroid and cholesterol metabolism involves both the ER and mitochondria, and a prior study has shown that mtDNA replication is “licensed” at mitochondria-ER contact sites[50], suggesting a potential connection between steroid and cholesterol metabolism and mtDNA CN. The specificity of the mtDNA CN increase to HEK293T cells may potentially be attributed to HEK293 adrenal lineage[37].

Discussion

Glucose deprivation sets off a complex series of adaptations to keep cells alive, including breakdown of glutamine, a shift to an oxidative metabolism, sequestration of cytosolic RNAs, and inhibition of cytosolic translation except for a select set of stress-related messenger RNAs[16,51–53]. Here, we add to this complex picture by showing that mitochondria respond by reducing transcription of their genome and stabilizing mtRNAs to maintain steady pools of mtRNA, a phenotype that is quickly reversed with re-introduction of glucose (Figs. 1A, 2B-C, and 3B-C).

The reduction in mitochondrial transcription rate in response to glucose deprivation is rapid, as we noted a drop in mtRNA synthesis to ~50% compared to HG after 90 min, with the slower mtRNA synthesis sustained at 12 h (Figs. 3B, 4B, and 6F). Importantly, we found that mitochondrial [ATP] was lower in glucose deprivation conditions compared to HG and closely mirrored mitochondrial transcription rate across this timeline. This, combined with reliance on OXPHOS (Fig. 1C and 6F), points to an upregulated mitochondrial ATP export when glycolysis does not produce ATP and argues that mitochondrial transcription rate can be predicted based on the energetic status of the cell. The recovery in mtRNA turnover upon glucose reintroduction points towards a synchronized adjustment in the rates of mtRNA synthesis and degradation. We noted brighter MRGs under glucose deprivation and a slower “chase” of BrU-labeled mtRNAs (Fig. 3A and 3B); however, mtRNAs were still being processed (Fig. S2D), pointing towards a potential slowing of mtRNA movement out of MRGs and accumulation of BrU-tagged RNAs in these granules. Additionally, the components of the mitochondrial

degradosome also still localized to mitochondria (Fig. S4B) and preserved their activity (e.g., SUV3 in Fig. S5C), suggesting that all stages of an mtRNA lifecycle are sustained under glucose deprivation but slowed.

We propose a flux-based model for regulation of mtRNA kinetics in response to nutrient availability (Fig. 7). During nutrient abundance, mtRNAs are overproduced (compared to the nuclear-encoded OXPHOS mRNAs) and passed to a system of mitochondrial bodies (MRGs, ribosomes, and degradosome) with finite pools of proteins in them. We propose that the proteins in these bodies are limiting, allowing excess mature RNAs are left behind to be degraded (Fig. 7A). Under nutrient deprivation, ATP-dependent mtRNA synthesis slows down, producing fewer “excess” mtRNAs and matching more closely the finite protein capacity of the mtRNA bodies. Excessive mtRNA transcription could thus be an adaptive process that acts as a buffer to cellular insults while metabolism adjusts to allow the cell to survive those insults.

Figure 7.

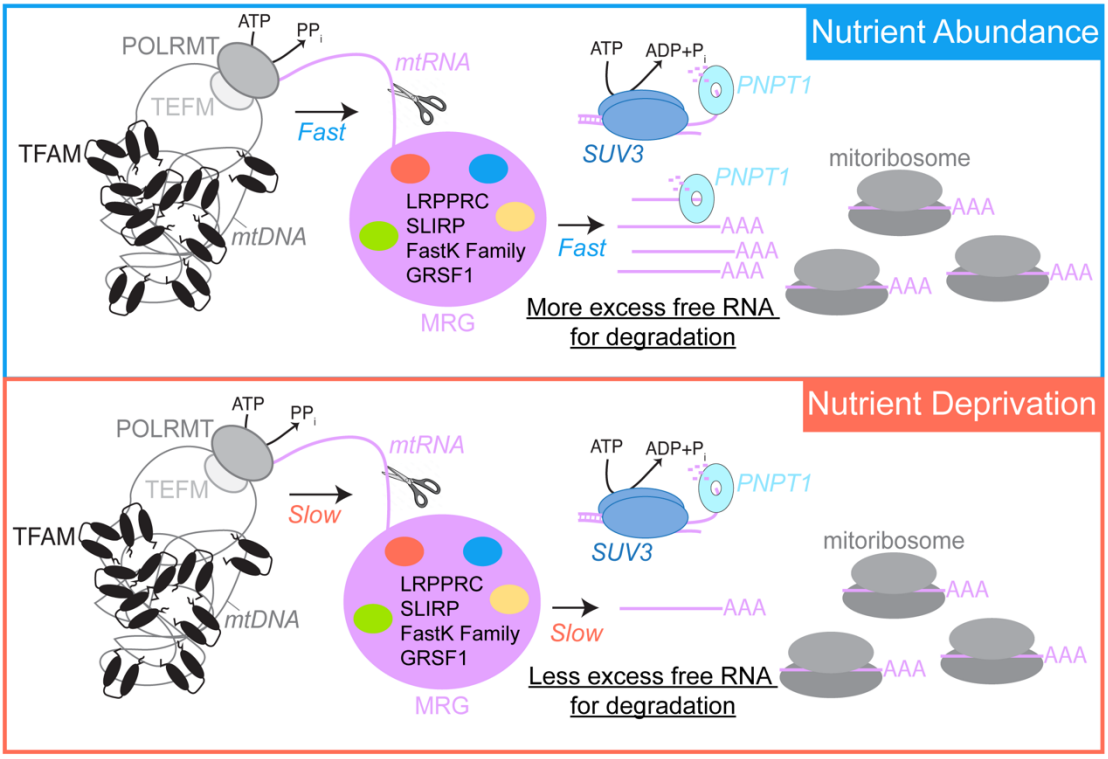

Figure 7. A flux-based model of mitochondrial gene expression changes under glucose deprivation. Overproduction of mitochondrial RNAs and movement through the mitochondrial RNA granule (MRG) in nutrient abundance leads to faster degradation rates (top), while slowing these processes during nutrient deprivation leads to less excess mtRNA produced and longer mtRNA lifetimes.

Our data differ from two recent studies showing new “bodies” formed by mtRNA under stress: one showing mitochondrial mRNA sequestered during long-term mitochondrial transcription inhibition with ethidium bromide or IMTB1[54], and another demonstrating that long-term SUV3 ablation leads to formation of distinct foci containing dsRNA and mitochondrial rRNA[31]. We believe the lack of these phenotypes in our experiments is due to the harshness of the insult in each study, in which specific parts of the mtRNA life cycle were inhibited during nutrient excess, therefore not showing a concerted shift across all parts of the mtRNA lifecycle. In contrast, our data show that an

intact mitochondrial central dogma can quickly adapt to an insult like nutrient deprivation without forming distinct mtRNA stress bodies. This work compliments a recent study in which ISR activation and subsequent cytosolic translation inhibition were shown to selectively allow local continued translation of mitochondrial proteins[55]. Our model predicts that the mitochondrial transcription system would be adapting to a slowed state to match this response.

Materials and Methods

In Progress…

ACKNOWLEDGEMENTS

We would like to thank the Debuloshina, Budin, Herzik, McHugh, Manor, and Zid labs for sharing materials, cell line, equipment, and expertise. We would like to thank Drs. Gerald S. Shadel, Brian M. Zid, Uri Manor, and L. Stirling Churchman, as well as the Mishanina and Churchman labs for insightful discussion. We would like to thank Julian Cicero of the Manor Lab for differentiation of the neural spheroid culture. RNA sequencing was conducted at the IGM Genomics Center, University of California, San Diego, La Jolla. We want to thank members of the UC San Diego School of Medicine Imaging Core: Jennifer Santini and Marcy Erb, as well as Carlos Alonso for guidance with confocal and STED imaging. The UC San Diego School of Medicine Imaging Core is supported by the NINDS P30NS047101 grant.

1. Soto, I. *et al.* Balanced mitochondrial and cytosolic translatomes underlie the biogenesis of human respiratory complexes. *Genome Biol.* **23**, 1–24 (2022).
2. Isaac, R. S., McShane, E. & Churchman, L. S. The multiple levels of mitonuclear coregulation. *Annu. Rev. Genet.* **52**, 511–533 (2018).
3. Gustafsson, C. M., Falkenberg, M. & Larsson, N. G. Maintenance and Expression of Mammalian Mitochondrial DNA. *Annu. Rev. Biochem.* **85**, 133–160 (2016).
4. Agaronyan, K., Morozov, Y. I., Anikin, M. & Temiakov, D. Replication-transcription switch in human mitochondria. *Science* **347**, 548–551 (2015).
5. Hillen, H. S., Temiakov, D. & Cramer, P. Structural basis of mitochondrial transcription. *Nat. Struct. Mol. Biol.* **25**, 754–765 (2018).
6. Ramachandran, A., Basu, U., Sultana, S., Nandakumar, D. & Patel, S. S. Human mitochondrial transcription factors TFAM and TFB2M work synergistically in promoter melting during transcription initiation. *Nucleic Acids Res.* **45**, 861–874 (2017).
7. Brüser, C., Keller-Findeisen, J. & Jakobs, S. The TFAM-to-mtDNA ratio defines inner-cellular nucleoid populations with distinct activity levels. *Cell Rep.* **37**, (2021).
8. Kukat, C. *et al.* Cross-strand binding of TFAM to a single mtDNA molecule forms the mitochondrial nucleoid. *Proc. Natl. Acad. Sci. U. S. A.* **112**, 11288–11293 (2015).
9. Farge, G. É. R. & Falkenberg, M. Organization of DNA in mammalian mitochondria. *Int. J. Mol. Sci.* **20**, 1–14 (2019).
10. Bonekamp, N. A. *et al.* High levels of TFAM repress mammalian mitochondrial DNA transcription in vivo. *Life Sci. Alliance* **4**, e202101034 (2021).
11. Rey, T. *et al.* Mitochondrial RNA granules are fluid condensates positioned by membrane dynamics. *Nat. Cell Biol.* **22**, 1180–1186 (2020).
12. McShane, E. *et al.* A kinetic dichotomy between mitochondrial and nuclear gene expression processes. *Mol. Cell* **84**, 1541-1555.e11 (2024).
13. Jain, M. *et al.* Dimeric assembly of human Suv3 helicase promotes its RNA unwinding function in mitochondrial RNA degradosome for RNA decay. *Protein Sci.* **31**, e4312 (2022).

14. Kühl, I. *et al.* POLRMT regulates the switch between replication primer formation and gene expression of mammalian mtDNA. *Sci. Adv.* **2**, e1600963 (2016).
15. Chang, D. D. & Clayton, D. A. Priming of human mitochondrial DNA replication occurs at the light-strand promoter. *Proc. Natl. Acad. Sci.* **82**, 351–355 (1985).
16. Balsa, E. *et al.* ER and Nutrient Stress Promote Assembly of Respiratory Chain Supercomplexes through the PERK-eIF2α Axis. *Mol. Cell* **74**, 877-890.e6 (2019).
17. Cox, P. J. & Clarke, K. Acute nutritional ketosis: implications for exercise performance and metabolism. *Extreme Physiol. Med.* **3**, 17 (2014).
18. George, F. C. Fuel metabolism in starvation. *Annu. Rev. Nutr.* **26**, 1–22 (2006).
19. Conte, F., Van Buuringen, N., Voermans, N. C. & Lefeber, D. J. Galactose in human metabolism, glycosylation and congenital metabolic diseases: Time for a closer look. *Biochim. Biophys. Acta BBA - Gen. Subj.* **1865**, 129898 (2021).
20. Bredvik, K., Liu, C. & Ryan, T. A. Characterization of β-Hydroxybutyrate as a Cell Autonomous Fuel for Active Excitatory and Inhibitory Neurons. Preprint at https://doi.org/10.1101/2024.06.08.598077 (2024).
21. Starck, S. R. *et al.* Translation from the 5′ untranslated region shapes the integrated stress response. *Science* **351**, aad3867 (2016).
22. Novoa, I. *et al.* Stress-induced gene expression requires programmed recovery from translational repression. *EMBO J.* **22**, 1180–1187 (2003).
23. Johnson, M. A. *et al.* Amino Acid Starvation Has Opposite Effects on Mitochondrial and Cytosolic Protein Synthesis. *PLoS ONE* **9**, e93597 (2014).
24. Watson, M. J. & Thoreen, C. C. Measuring mRNA Decay with Roadblock-qPCR. *Curr. Protoc.* **2**, e344 (2022).
25. Burger, K. *et al.* 4-thiouridine inhibits rRNA synthesis and causes a nucleolar stress response. *RNA Biol.* **10**, 1623–1630 (2013).
26. Mennuni, M. *et al.* Metabolic resistance to the inhibition of mitochondrial transcription revealed by CRISPR-Cas9 screen. *EMBO Rep.* **23**, e53054 (2022).

27. Zhu, X. *et al.* Non-coding 7S RNA inhibits transcription via mitochondrial RNA polymerase dimerization. *Cell* 1–15 (2022) doi:10.1016/j.cell.2022.05.006.
28. Hansen et al. - 2024 - Transcription arrest induces formation of protecti.pdf.
29. Begeman et al. - 2024 - A spatial atlas of mitochondrial gene expression r.pdf.
30. Marvin, J. S. *et al.* iATPSnFR2: A high-dynamic-range fluorescent sensor for monitoring intracellular ATP. *Proc. Natl. Acad. Sci.* **121**, e2314604121 (2024).
31. Begeman, A., Smolka, J. A., Shami, A., Waingankar, T. P. & Lewis, S. C. Spatial analysis of mitochondrial gene expression reveals dynamic translation hubs and remodeling in stress. *C E N C E V N C E S* (2025).
32. Kurtoglu, M., Maher, J. C. & Lampidis, T. J. Differential Toxic Mechanisms of 2-Deoxy-D-Glucose *versus* 2-Fluorodeoxy-D -Glucose in Hypoxic and Normoxic Tumor Cells. *Antioxid. Redox Signal.* **9**, 1383–1390 (2007).
33. Chen, W. & Gu, M. The inhibition of bovine heart hexokinase by 2-deoxy-D-glucose-6-phosphate: characterization by alp NMR and metabolic implications.
34. Winther, A.-M. L. *et al.* Critical Roles of Hydrophobicity and Orientation of Side Chains for Inactivation of Sarcoplasmic Reticulum Ca2+-ATPase with Thapsigargin and Thapsigargin Analogs. *J. Biol. Chem.* **285**, 28883–28892 (2010).
35. Sehgal, P. *et al.* Inhibition of the sarco/endoplasmic reticulum (ER) Ca2+-ATPase by thapsigargin analogs induces cell death via ER Ca2+ depletion and the unfolded protein response. *J. Biol. Chem.* **292**, 19656–19673 (2017).
36. Kaspar, S. *et al.* Adaptation to mitochondrial stress requires CHOP-directed tuning of ISR. *Sci. Adv.* **7**, (2021).
37. Lin, Y.-C. *et al.* Genome dynamics of the human embryonic kidney 293 lineage in response to cell biology manipulations. *Nat. Commun.* **5**, 4767 (2014).
38. Boulwareo, S. D., Mason, G. F., Shulman, G. I., Shulman, R. G. & TAMBORLANEt, W. V. D13i(rCeNctMmReasspuecrtermoesnctopoyf brain glucose concentrations in humans by.

39. García-Villegas, R. *et al.* In vivo composition of the mitochondrial nucleoid in mice. *Biochim. Biophys. Acta BBA - Mol. Cell Res.* **1872**, 119955 (2025).
40. Qin, J. *et al.* Ketogenic diet reshapes cancer metabolism through lysine β-hydroxybutyrylation. *Nat. Metab.* **6**, 1505–1528 (2024).
41. Tsusaka, T. *et al.* Reversible histone deacetylase activity catalyzes lysine acylation. *Nat. Chem. Biol.* (2025) doi:10.1038/s41589-025-01869-5.
42. Xie, Z. *et al.* Metabolic Regulation of Gene Expression by Histone Lysine β-Hydroxybutyrylation. *Mol. Cell* **62**, 194–206 (2016).
43. Yang, T. *et al.* Crucial Step in Cholesterol Homeostasis: Sterols Promote Binding of SCAP to INSIG-1, a Membrane Protein that Facilitates Retention of SREBPs in ER.
44. Clizbe, D. B., Owens, M. L., Masuda, K. R., Shackelford, J. E. & Krisans, S. K. IDI2, a Second Isopentenyl Diphosphate Isomerase in Mammals. *J. Biol. Chem.* **282**, 6668–6676 (2007).
45. Hunter, A. L. *et al.* Adipocyte NR1D1 dictates adipose tissue expansion during obesity. *eLife* **10**, e63324 (2021).
46. Bansal, S. *et al.* Mitochondrial Targeting of Cytochrome P450 (CYP) 1B1 and Its Role in Polycyclic Aromatic Hydrocarbon-induced Mitochondrial Dysfunction. *J. Biol. Chem.* **289**, 9936–9951 (2014).
47. Lin, Y. C., Cheung, G., Zhang, Z. & Papadopoulos, V. Mitochondrial cytochrome P450 1B1 is involved in pregnenolone synthesis in human brain cells. *J. Biol. Chem.* **299**, 105035 (2023).
48. Dussossoy, D. *et al.* Colocalization of sterol isomerase and $sigma_1$ receptor at endoplasmic reticulum and nuclear envelope level. *Eur. J. Biochem.* **263**, 377–386 (1999).
49. Gomez, A. *et al.* Characterization of TCDD-inducible poly-ADP-ribose polymerase (TIPARP/ARTD14) catalytic activity. *Biochem. J.* **475**, 3827–3846 (2018).
50. Lewis, S. C., Uchiyama, L. F. & Nunnari, J. ER-mitochondria contacts couple mtDNA synthesis with Mitochondrial division in human cells. *Science* **353**, (2016).

51. Zhang et al. - 2020 - Glucose Starvation Blocks Translation at Multiple .pdf.
52. Jain et al. - 2016 - ATPase-Modulated Stress Granules Contain a Diverse.pdf.
53. Rossignol et al. - 2004 - Energy Substrate Modulates Mitochondrial Structure.pdf.
54. Hansen, K. G., Baxter-Koenigs, A., Weiss, C. A. M., McShane, E. & Stirling Churchman, L. Transcription arrest induces formation of protective RNA granules in mitochondria. Preprint at https://doi.org/10.1101/2024.09.25.614902 (2024).
55. Brar, K. K. *et al.* PERK-ATAD3A interaction provides a subcellular safe haven for protein synthesis during ER stress. *Science* **385**, eadp7114 (2024).
56. Bolger et al. - 2014 - Trimmomatic a flexible trimmer for Illumina seque.pdf.
57. Dobin et al. - 2013 - STAR ultrafast universal RNA-seq aligner.pdf.
58. Love et al. - 2014 - Moderated estimation of fold change and dispersion.pdf.
59. Kuleshov et al. - 2016 - Enrichr a comprehensive gene set enrichment analy.pdf.
60. Rath, S. *et al.* MitoCarta3.0: an updated mitochondrial proteome now with sub-organelle localization and pathway annotations. *Nucleic Acids Res.* **49**, D1541–D1547 (2021).
61. Watson and Thoreen - 2022 - Measuring mRNA Decay with Roadblock-qPCR.pdf.
62. Jourdain, A. A. *et al.* GRSF1 regulates RNA processing in mitochondrial RNA granules. *Cell Metab.* **17**, 399–410 (2013).

Supplemental Figure 1

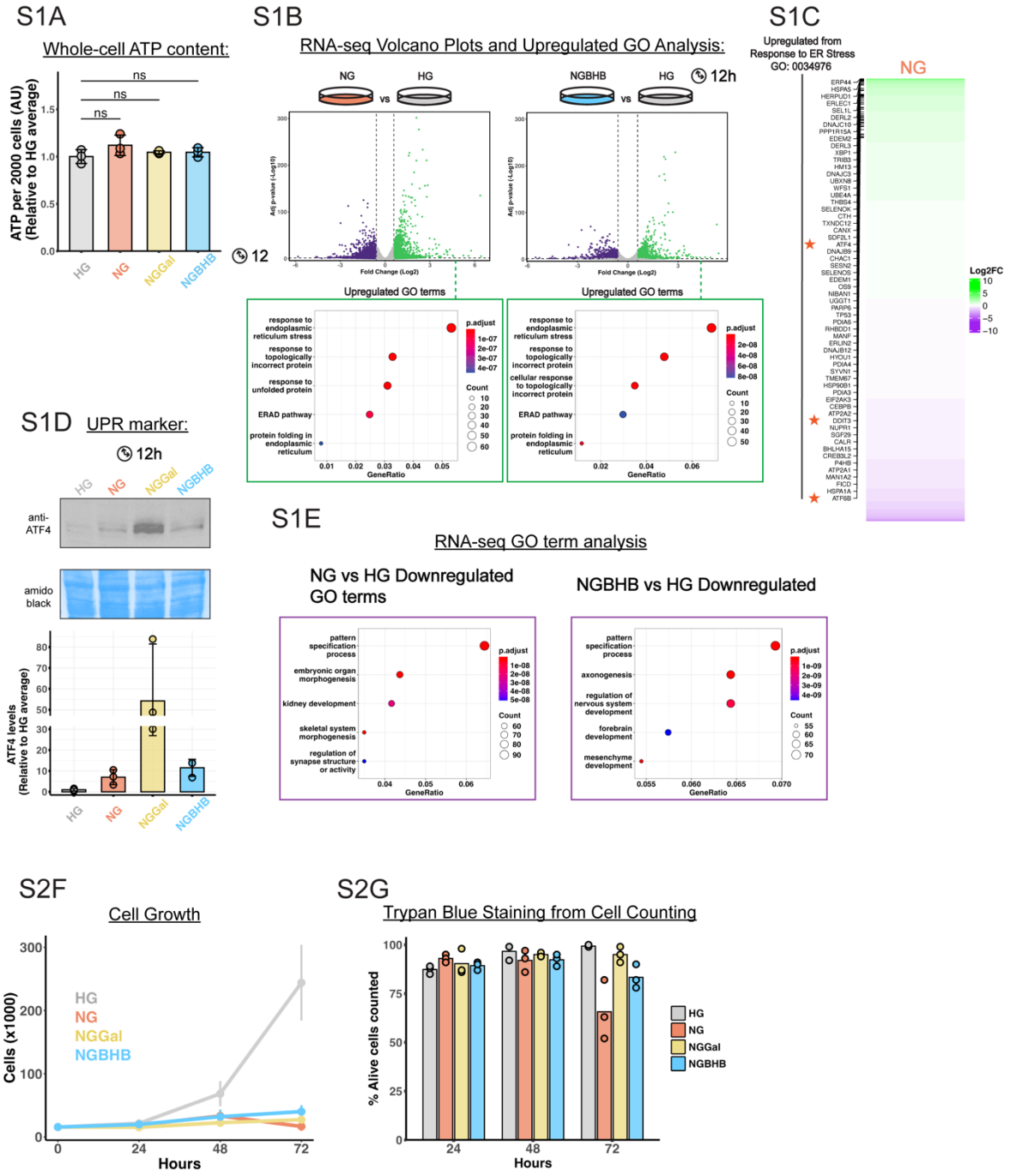

Supplemental Figure 1

S1H

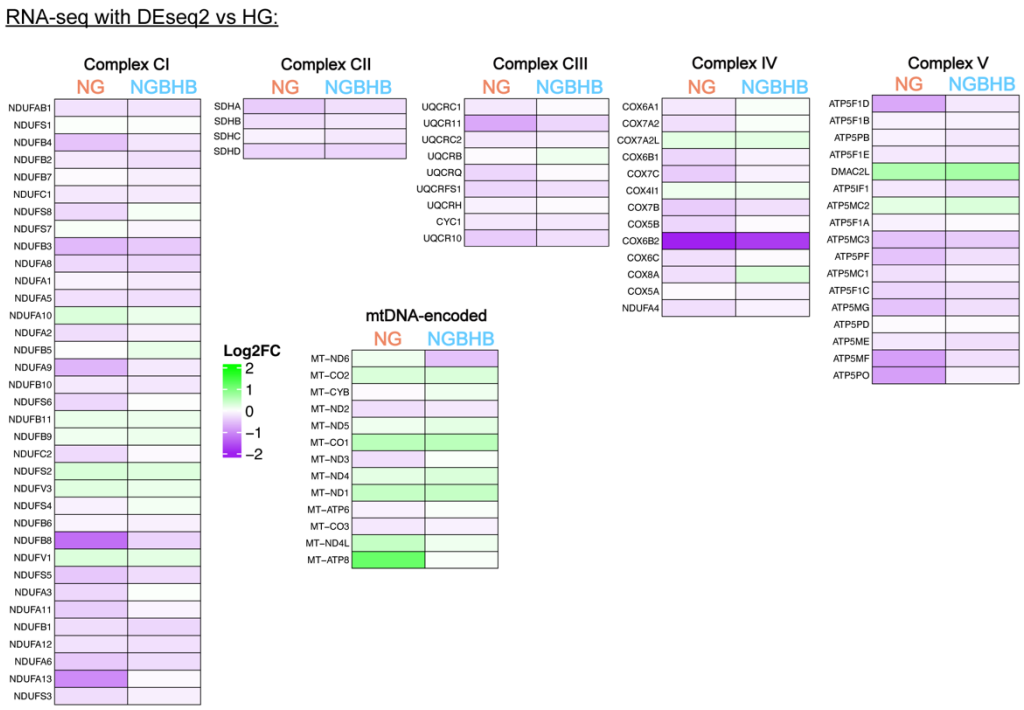

S1F

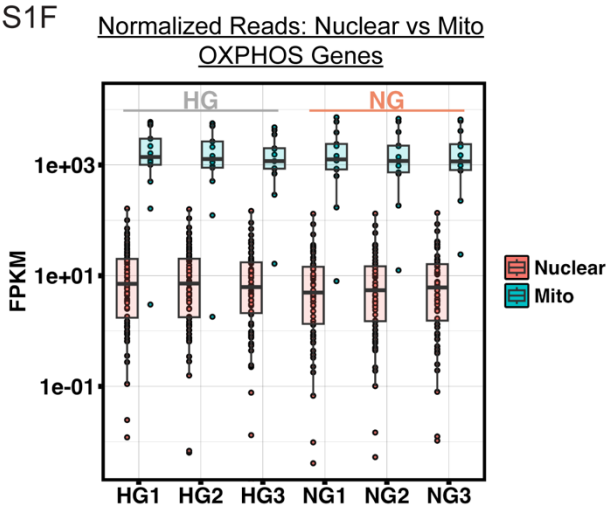

Supplemental Figure 1. A) Whole-cell ATP content measurements with an ATP GLOW assay in cells deprived of glucose for 12 h (ns, non-significant; one-way ANOVA with Tukey's multiple comparisons correction, data are means ± S.D.). **B)** RNA-seq volcano plots depicting differential gene expression analysis following 12 h treatments, with upregulated genes in green and downregulated genes in purple. Gene ontology (GO)

analysis of upregulated genes from each dataset is shown in the bottom panels. Genes were considered “differentially expressed” if they showed fold changes >1.3 and adjusted p-value <0.05 (n = 3 biological replicates). **C)** Genes analyzed for gene expression analysis in NG vs HG with upregulated genes associated with the response to ER Stress (GO:0034976) shown to the left, and specific ISR transcription factors marked with orange stars. **D)** A representative western blot (top) showing ATF4 protein levels in glucose-deprived HEK293T cells, quantified (bottom) and normalized to high glucose (HG) average from 3 independent biological experiments. **E)** Gene ontology (GO) analysis of downregulated genes from transcriptomics comparing HEK293T cells 12 h treated NGGal and NGBHB compared to HG. (n = 3 biological replicates). **F)** Cell counting for HEK293T cells treated for 24, 48, and 72 hours in high glucose (HG), no glucose (NG), no-glucose-galactose (NGGal), and no-glucose-beta-hydroxybutyrate (NGBHB) (n = 3 biological replicates). **G)** Cell survival percentage determined by Trypan Blue staining from cells counted in F. **H)** Heatmap showing RNA-seq based $\log_2$ fold-change in expression of nuclear and mitochondrially encoded OXPHOS protein genes after a 12 h NG or NGBHB treatment, compared to HG (n = 3 biological replicates) **F)** RNA-seq analysis of nuclear and mitochondrially encoded OXPHOS protein genes as FPKM (n = 3 biological replicates).

Supplemental Figure 2

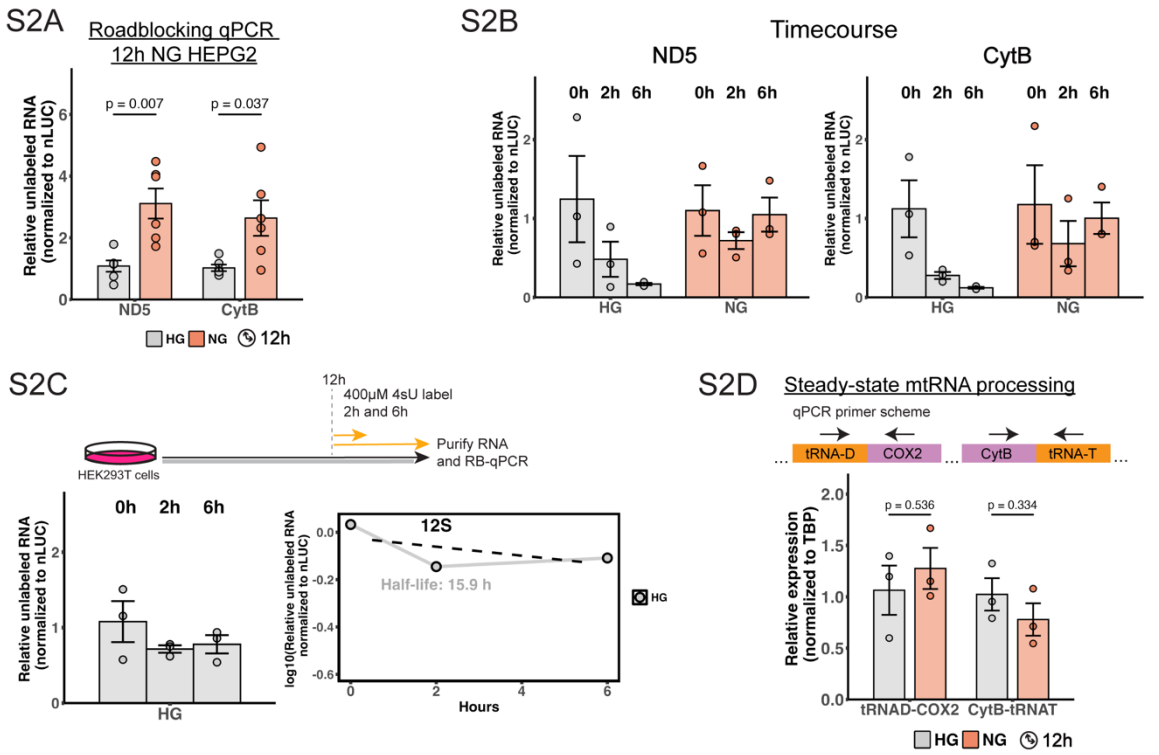

Supplemental Figure 2: A) Roadblocking qPCR analysis for HEPG2 cells treated for 12 h in high glucose (HG) or no-glucose (NG) (n = 6 biological replicates, two-tailed Student's *t*-test, data is mean ± s.e.m. with associated *P* values). **B)** Roadblocking qPCR analysis for ND5 and CytB in HEK293T cells treated with HG or NG for 12 h before 4sU incorporation for 0, 2, or 6 h (n = 3 biological replicates, normalized to nLUC RNA and the respective 0 h timepoint). **C)** Roadblocking qPCR analysis for the mitochondrial 12S ribosomal RNA (12S RNA) in HEK293T cells treated with HG for 12 h before 4sU incorporation for 0, 2, or 6 h (n = 3 biological replicates, normalized to nLUC RNA and the respective 0 h timepoint). **D)** Scheme and quantification for qPCR analysis of mitochondrial RNA processing in HEK293T cells treated in NG for 12 h compared to HG (n = 3 biological replicates, normalized to tata-box-binding protein (TBP), two-tailed Student's *t*-test, data is mean ± s.e.m. with associated *P* values).

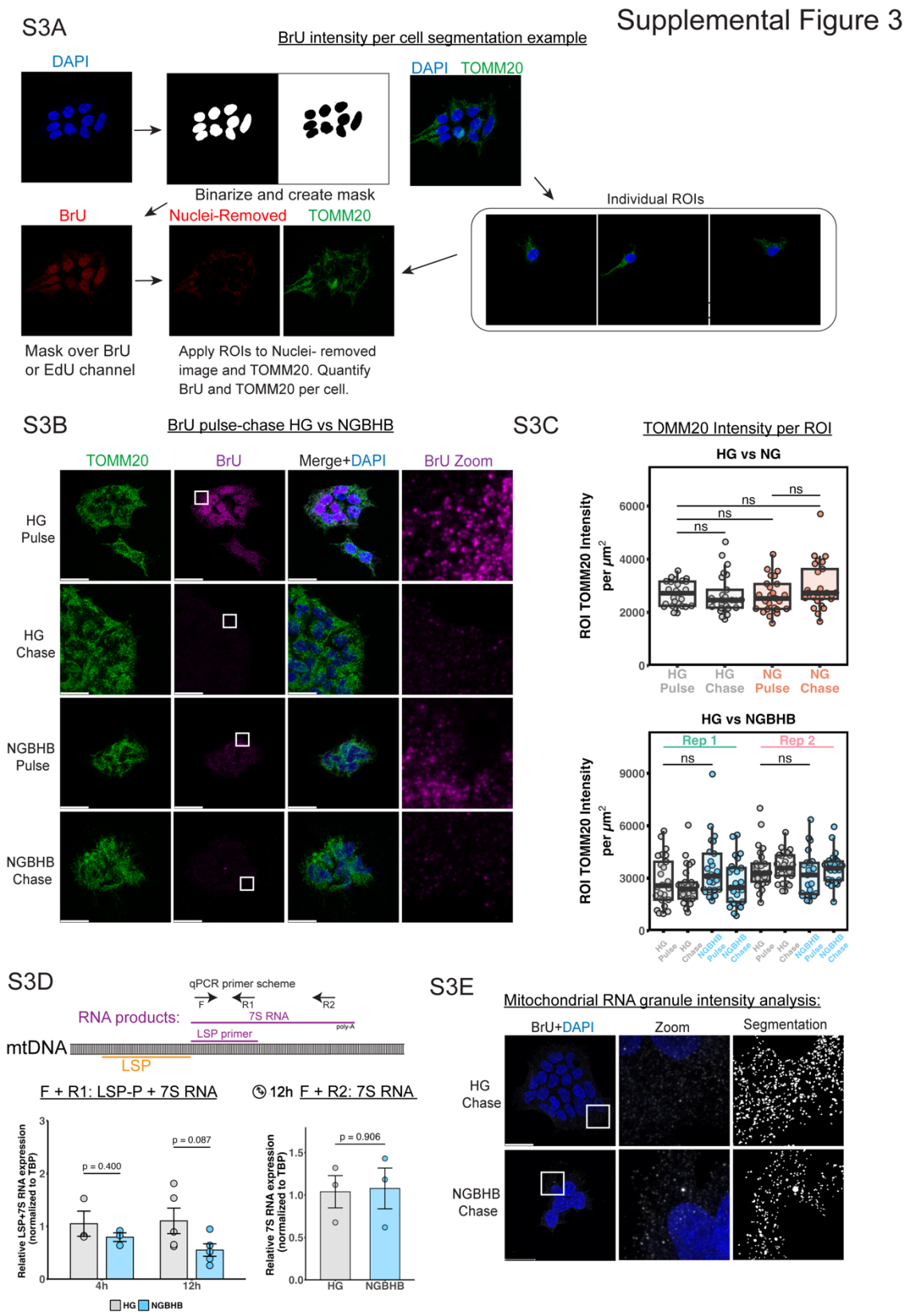

Supplemental Figure 3: A) Example segmentation scheme for measurement of

extranuclear BrU or EdU intensity in HEK 293T cells. This includes nucleus removal and ROI selection to represent individual cells. **B)** Representative images as maximum intensity projections for HG vs. NGBHB treated cells stained against TOMM20 (mitochondria) and BrU (newly synthesized RNA). Scale bar = 30 μm. **C)** Quantification of TOMM20 intensity per cell ROI for pulse and chase samples of HG vs NG (top), and HG vs. NGBHB (bottom, ns, non-significant; one-way ANOVA with Tukey's multiple comparisons correction; n=50 cells per replicate, with 25 cells in each condition quantified, data represents individual cells and bars represent median, boxes represent the 1st and 3rd quartiles, and whiskers are no further than 1.5 times the interquartile range). **D)** Quantitative PCR (qPCR) primer scheme and analysis of the mitochondrial Light Strand Promoter primer region and 7S RNA in HEK293T cells treated for 12 h in HG or NGBHB (n = 3-6 biological replicates, normalized to tata-box-binding protein (TBP), two-tailed Student's *t*-test, data is the mean ± s.e.m. and associated *P* value). **E)** Maximum intensity projection chase images for HG and NGBHB treated cells, and segmented mitochondrial RNA granules (left, MRGs) for quantification of average pixel intensity per MRG from samples in 3B (right).

Supplemental Figure 4

S4A

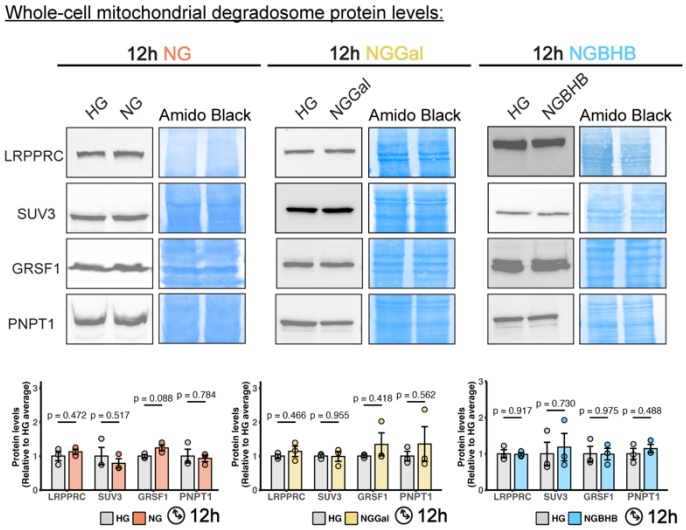

S4B

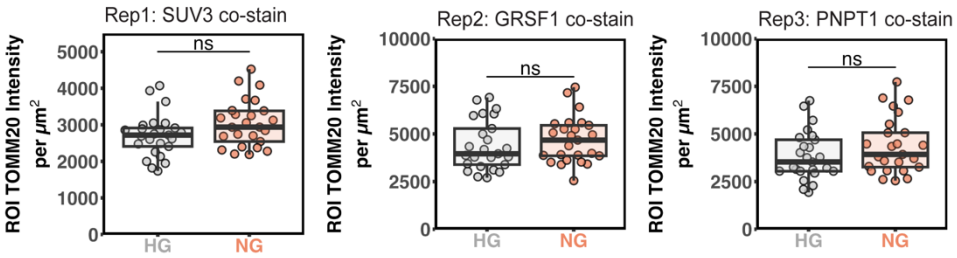

Supplemental Figure 4: A) Quantification of TOMM20 intensity per cell ROI for 12 h NG pulse samples described in and chase samples of HG vs NG (top), and HG vs. NGBHB (ns, non-significant; two-tailed Student's *t*-test; n=50 cells per replicate, with 25 cells in each condition quantified, data represents individual cells and bars represent median, boxes represent the 1st and 3rd quartiles, and whiskers are no further than 1.5 times the interquartile range).

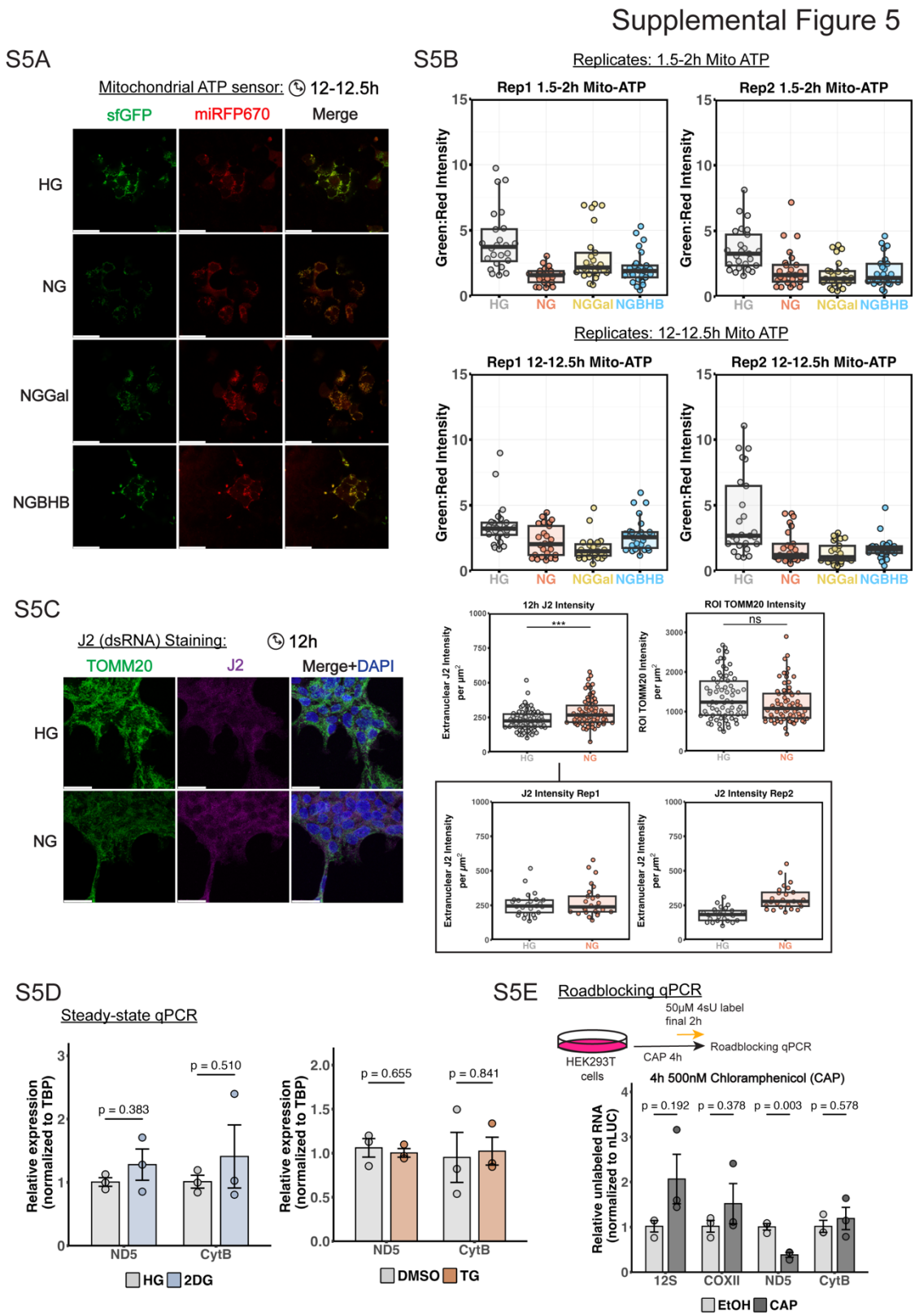

Supplemental Figure 5: A) Representative 2D images of mitochondrial ATP sensor imaging in HEK293T cells during treatment for 12 h hours with glucose deprivation

conditions. **B)** Replicate data for quantification of mitochondrial ATP per cell as the ratio of green:red intensity for samples treated in each condition for 1.5 and 12 h in Fig. 5B. Data represents individual cells and bars represent median, boxes represent the 1st and 3rd quartiles, and whiskers are no further than 1.5 times the interquartile range. **C)** Representative images of extranuclear dsRNA immunostaining with the J2 antibody of HEK293T cells treated with NG for 12 h. Cells were stained against TOMM20 (green, mitochondria) and J2 (magenta, dsRNA). **D)** Quantification of extranuclear dsRNA (J2) intensity and TOMM20 intensity per cell ROI from cells in S5C (top)(ns, non-significant ; ***$p<0.001$, two-tailed Student's *t*-test; n=60 cells per condition, with 30 cells in each condition quantified per replicate, data represents individual cells and bars represent median, boxes represent the 1st and 3rd quartiles, and whiskers are no further than 1.5 times the interquartile range). Replicate data for J2 measurements are boxed (below). **E)** Quantitative PCR (qPCR) analysis of representative mitochondrial transcripts shows steady pools of these RNAs after treatment with 25mM 2DG or 1μM thapsigargin (n = 3 biological replicates, normalized to tata-box-binding protein (TBP), data are means ± S.E.M. and associated *p* values). **F)** Roadblocking qPCR analysis for HEK293T cells treated for 12 h with 500nM chloramphenicol (n = 3 biological replicates, two-tailed Student's *t*-test, data is mean ± s.e.m. with associated *P* values).

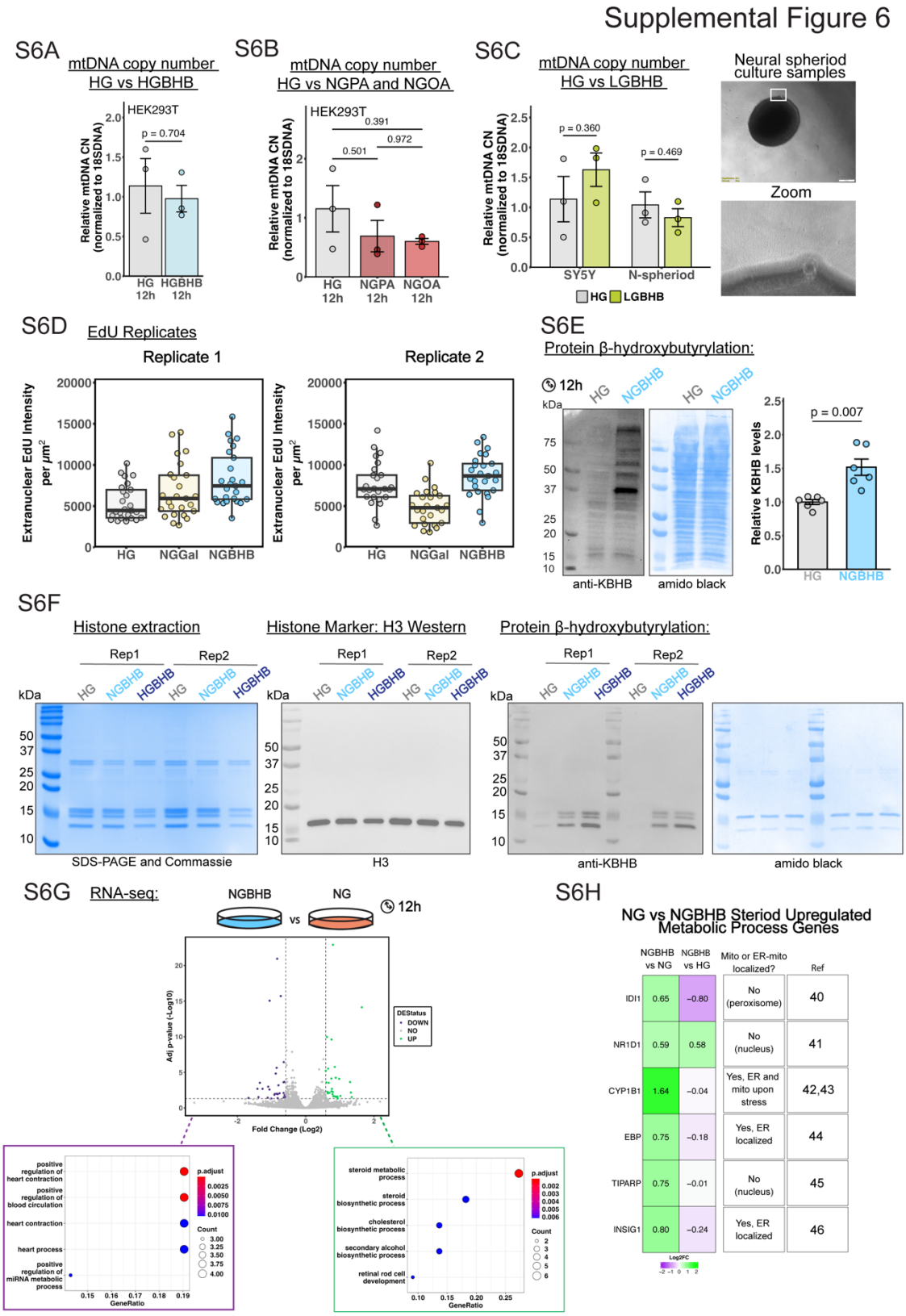

Supplemental Figure 6: A) Quantitative PCR (qPCR) analysis of mitochondrial DNA copy number between 12 h high glucose (HG) and high-glucose-betahydroxybutyrate

(HGBHB) treated HEK293T. Mitochondrial DNA was detected with primers for CytB normalized to 18S DNA (n = 3 biological replicates, two-tailed Student's *t*-test, data is mean ± s.e.m. with associated *P* values). **B)** Quantitative PCR (qPCR) analysis of mitochondrial DNA copy number between high glucose (HG) and no-glucose-palmitic acid (PA) and no-glucose-oleic-acid (OE) conditions in HEK293T cells treated for 12 h. mtDNA was detected as above (n = 3 biological replicates, two-tailed Student's *t*-test, data is mean ± s.e.m. with associated *P* values). **C)** Quantitative PCR (qPCR) analysis of mitochondrial DNA copy number between high glucose (HG) and low-glucose-beta-hydroxybutyrate (LGBHB) conditions in SH-SY5Y cells and human neuronal spheroid culture treated for 12 h. (left, n = 3 biological replicates, two-tailed Student's *t*-test, data is mean ± s.e.m. with associated *P* values) and images of human neuronal spheroid culture showing axons (right). **D)** Replicate data for the quantification of extranuclear EdU intensity per HEK293T cell in EdU pulse samples of high glucose (HG), no-glucose-galactose (NGGal), and no-glucose-BHB (NGBHB) treated cells (25 cells per condition and replicate, points represent individual cells, data represents individual cells and bars represent median, boxes represent the 1st and 3rd quartiles, and whiskers are no further than 1.5 times the interquartile range). **E)** Western blot analysis of lysine beta-hydroxybutyrylation (KBHB) from HEK293T cell lysate treated with HG or NGBHB for 12 h (top), and quantification of blots (below, n = 6 biological replicates, normalized to high glucose (HG) average value, two-tailed Student's *t*-test with associated *P* values). **F)** SDS-PAGE gel for cell fractionation and histone extraction from HEK293T cells treated with HG, NGBHB, and HGBHB for 12 h (left), Histone H3 western blots of these samples (center-left), KBHB western blots of these samples (center-right), and amido black staining of the KBHB western blot (right). **G)** Volcano plots depicting differential gene expression analysis between HEK293T cells treated for 12 h in NGBHB or NG, with upregulated (green), downregulated genes (purple), and gene ontology (GO) analysis of upregulated genes from each dataset (bottom) shown. Genes were considered "differentially expressed" if they had fold changes >1.3 and adjusted p-value <0.05 (n = 3 biological replicates). **H)** Log-2 fold-change data from differential gene expression analysis for upregulated genes related to the "steroid metabolic process" GO term in HEK293T cells from 12 h NGBHB vs 12 h NG treatment (n = 3 biological replicates).